



Cite this: DOI: 10.1039/d1ce00234a

Spin crossover crystalline materials engineered via single-crystal-to-single-crystal transformations

 Shufang Xue, ^a Yunnan Guo ^{*a} and Yann Garcia ^{*b}

Spin crossover continues to stimulate multidisciplinary research efforts worldwide as novel potential applications of its intrinsic molecular bistability property are envisaged. The challenge of mastering the switchable capability for its exploitation belongs largely to the realm of chemical design and synthesis. In this respect, single-crystal-to-single-crystal (SCSC) transformations as an effective engineering alternative method have attracted considerable attention in the design of specific spin crossover materials. However, spin state switching in a SCSC fashion between discrete molecular crystals has been limited, since crystals can hardly retain single crystallinity when they suffer from external stimuli. This highlight illustrates the latest crystalline materials engineered via SCSC transformations, with emphasis on the onset and progress of spin crossover in a crystal control.

 Received 17th February 2021,
 Accepted 27th April 2021

DOI: 10.1039/d1ce00234a

rsc.li/crystengcomm

1. Introduction

Spin crossover (SCO) phenomena exhibited by some octahedral $3d^4$ to $3d^7$ transition metals continue to stimulate multidisciplinary research efforts worldwide as novel potential applications of molecular bistability are envisaged.^{1–4} The bistability arises from their hysteresis loops as a result of their switchable ability between two electronic states – high-spin (HS) and low-spin (LS) – by external stimuli (temperature, pressure, light or solvent), in a readily detectable and reversible way.^{5,6} So far, the challenge of mastering the switchable capability for its exploitation belongs largely to the realm of chemical design and synthesis. The ideal switching features rely on a good control of the cooperativity and enhancement of transition temperature ($T_{1/2}$). In essence, SCO behaviour incorporating hysteresis phenomenon is dependent on the cooperativity, that is how individual SCO centres interact, both intramolecularly and intermolecularly,⁷ by virtue of elastic contacts involving hydrogen bonding (HB), halogen bonding (XB) as well as $\pi\cdots\pi$ interactions.^{8–11} Such cooperativity is key to control the shape and potential hysteresis width, *i.e.* resulting in a memory effect. Moreover, $T_{1/2}$ is largely dependent on the coordination sphere around the spin carrier. Great efforts have thus been devoted to the

rational design of ligands for the bridging of individual metal centres altogether with to manipulating the noncovalent interaction between different SCO units in the solid state by changing crystallization solvents or counter anions.^{7,12,13} The solvent molecule introduced during the synthesis often act as “chemical pressure” to affect the magnetic behaviour dramatically. From the standpoint of synthesis, various chemical and physical approaches have been successfully utilized to obtain SCO materials with hysteretic loops in various temperature regions. Of particular interest, engineering alternative methods of preparing SCO crystalline materials ideally involving a larger degree of rational design, is highly desirable.

In this respect, single-crystal-to-single-crystal (SCSC) transformations induced by external stimuli (temperature, light or solvent) have attracted considerable attention in the design of specific crystalline materials. The long-sought-after developments reveal that SCSC offer strategies to construct specific coordination compounds, especially solvent-free, solvent-partially-desolvated or the intermediate analogues that cannot be formed by conventional method and also to fabricate systems with enhanced functionalities and novel applications.¹⁴ Generally, SCSC transformations involve cooperative movement of atoms in the solid state accompanied by breaking and formation of coordinate and/or covalent bonds,¹⁵ to afford accurate imagery about structural alterations that can undoubtedly modulate magnetic properties.^{16,17} This is particularly reliable since a subtle perturbation in the metal–ligand environment can have a profound impact on the performance of the spin transition. Such fine-tune of SCO behaviour needs to satisfy the prerequisite that structural integrity remains intact after SCSC transformation. Notably, the

^a Department of Chemistry, Key Laboratory of Surface & Interface Science of Polymer Materials of Zhejiang Province, Zhejiang Sci-Tech University, Hangzhou 310018, China. E-mail: yunnanguo@zstu.edu.cn

^b Institute of Condensed Matter and Nanosciences, Molecular Chemistry, Materials and Catalysis (IMCN/MOST), Université catholique de Louvain, Place L. Pasteur 1, 1348 Louvain-la-Neuve, Belgium. E-mail: yann.garcia@uclouvain.be

Table 1 Transformation of structures and magnetic properties via SCSC process

Starting complex	SCSC process	Transformed complex	Structural transformation	Change of SCO profile	$T_{1/2}/K$		Ref.
					Starting complex	Transformed complex	
1	Reversible heat/H ₂ O	2	Solvent release, bond cleavage and formation and coordination environment change	One step \rightleftharpoons one step	202	160	28
3	Reversible heat/H ₂ O	4	Solvent release, bond cleavage and formation, dimensionality (0D \rightarrow 1D)	One step \rightleftharpoons two step	¹ 218 ¹ 222	\sim ¹ 275 \sim "200	32
5·3MeOH	Heat	5	Solvent release, crystal symmetry breaking ($P2_1/n \rightarrow C2/c$) and disorder of ligands	One step \rightarrow two step	135	¹ 181 ¹ 185 ¹ "141 ¹ "148	36
6·H ₂ O	Reversible heat/H ₂ O	6	Solvent release and crystal symmetry breaking ($I4_1/a \rightarrow P4_2/n$)	One step \rightleftharpoons two step	Incomplete	¹ 270 ¹ 287 ¹ "155 ¹ "195	37
7·3C ₃ H ₆ O	Heat	7	Solvent release and supramolecular interaction	HS \rightarrow LS	HS	LS	38
8·4H ₂ O	Heat	8	Solvent release and supramolecular isomerization (<i>cis</i> \rightarrow <i>trans</i>)	Half-SCO \rightarrow one step	Half-SCO	¹ 268.4 ¹ 269.7	39
10·2CH ₃ CN	Heat	10	Solvent release and supramolecular interaction	One step \rightarrow two step	350	\sim ¹ 250 \sim "200	45
11·3MeOH	Reversible heat/MeOH	11	Solvent release and supramolecular interaction	One step \rightleftharpoons HS	¹ 271 ¹ 273	HS	46
11·2H ₂ O	Reversible heat/H ₂ O	11	Solvent release and supramolecular interaction	One step \rightleftharpoons HS	269	HS	46
12·2H ₂ O	Reversible heat/H ₂ O	12	Solvent release and supramolecular interaction	One step \rightleftharpoons HS	125	HS	51
13·2H ₂ O	Reversible heat/H ₂ O	13	Solvent release and supramolecular interaction	LS \rightleftharpoons one step	LS	¹ 235 ¹ 267	52
14	MeOH vapor	14·MeOH	Supramolecular interaction	One step \rightarrow two step	Incomplete	¹ 303 ¹ 229	7
15·Et ₂ O	Reversible solvent vapor	15·3H ₂ O	Solvent exchange and supramolecular interaction	One step \rightleftharpoons two step	305	¹ 346 ¹ 326	60
18	Reversible heat/C ₃ H ₆ O	19	Solvent release, crystal symmetry breaking ($P2_1/n \rightarrow P1$), rotation of the ligands	LS \rightleftharpoons HS	LS	HS	58
19	Solvent vapor	19	Solvent exchange and supramolecular interaction	HS (19) \rightleftharpoons LS (19·MeOH, 19·EtOH, 19·PrOH)	HS	LS	54
20·MeOH	Reversible heat/MeOH	20	Supramolecular interaction (mixed HB/XB \rightleftharpoons XB)	One step \rightleftharpoons one step	205	270	67
20·H ₂ O	Reversible heat/H ₂ O	20	Supramolecular interaction (mixed HB/XB \rightleftharpoons XB)	One step \rightleftharpoons one step	300	270	67
21-I	Heat	21-II	Rotation of the BPh ₄ ⁻ anion	Gradual \rightarrow abrupt	270	¹ 229 ¹ 234	68
21-II	Reversible heat/vapor	21-III/21-IV	Rotation of the BPh ₄ ⁻ anion	Abrupt \rightleftharpoons abrupt	¹ 229 ¹ 234	¹ 221-III ¹ 234-III ¹ 225-IV ¹ 234-IV	68
26	Light	28	Photocyclization	LS \rightleftharpoons HS	LS	HS (30%) At 300 K	80
29	Light	29'	[2 + 2] cycloaddition	One step \rightarrow two step	¹ 212 ¹ 215	¹ 190 ¹ 194 ¹ "166 ¹ "169	82
30	Light	30'	[2 + 2] cycloaddition	Two step \rightarrow one step	¹ 190 ¹ 194 ¹ "166 ¹ "169	162	82
32	Cation exchange	32@33	Na ⁺ exchanged by Fe(sal ₂ -trien) ⁺	LS \rightarrow SCO	LS	SCO	94
35	Cation exchange	FeNi-3	Bond cleavage and formation	Paramagnetic behaviour \rightarrow SCO	Paramagnetic behaviour	SCO	98
36	Redox	36@I ₂	C=C bond of TTF	Incomplete \rightarrow incomplete LIESST \rightarrow none	Incomplete	Incomplete	101

reversible switching of a thermal hysteresis loop *via* a SCSC event reported in SCO frameworks is very attractive and widely investigated, since it takes advantage of robust polymeric networks of the hosts.^{9,18–21} However, while equally interesting, it is more rare to witness SCSC compositional changes in molecular materials due to the intrinsically larger challenge of retention of a single crystalline phase in a molecular solid. Although some reviews occasionally concern complexes showing SCO proceeding in a SCSC fashion,^{22,23} the work has not yet been reviewed. We therefore herein illustrate the latest crystalline materials engineered *via* SCSC transformations, with emphasis on the onset and progress of SCO in a crystal control (Table 1). The whole highlight has been divided into the following sections based on the origin of SCSC transformations: (i) solvent-induced transformations, (ii) light-induced transformations, (iii) cation-centre-exchange-induced transformations and (iv) redox-induced transformations.

2. Solvent-induced SCSC transformations

Solvent molecules are known to play an indispensable role in the crystallization process, acting as an effective and selective medium to fine-tune the polymorphism as well as to complete the coordination of a metal centre and/or to retain a crystalline phase in the lattice.¹² As solvent molecules have no strong coordination interaction with the metallic centre as the ligands, so removing or exchanging these molecules can be achieved by heating or through molecule exchange.²⁴

2.1. SCO induced by solvent-release transformation

Small solvent molecules in crystalline materials mainly existing in free and terminal coordinated forms, are easily removed under mild conditions (heating below 150 °C) for the formation of a desolvated phase to further modulate the SCO behaviour. Several phenomena accompanying solvent release have been identified, with alternation of the metal coordination environment, structural dimensionality, crystal symmetry, *cis-to-trans* transformation as well as supramolecular interactions.

Coordination environment. SCSC-induced alternation of the metal coordination environment is referred to ligand exchange *via* formation or cleavage of metal–ligand bonds.¹⁵ However, the process of ligand loss from a single crystal and reversible relegation is usually accompanied by decay of the single crystal to a microcrystalline powder.²⁵ One effective strategy is that ligand-exchange SCSC transformations *via* a gas–solid reaction involve the interchange of coordinated small ligands (MeOH (ref. 26) or H₂ (ref. 27)) at metal centre in molecular single crystals, whose crystals remain intact even after a solid-state rearrangement of atoms. Besides, it is of great potential that coordinated solvent molecule will be substituted by the counterion in the lattice during the SCSC desolvated process. As observed in a trinuclear Fe^{II} complex [Fe₃(NH₂-trz)₆(SCN)₄(H₂O)₂](SCN)₂·H₂O (**1**), where NH₂trz = 4-amino-1,2,4-triazole, a single crystal of **1** has an ability to extrude one lattice

water O₃ and one coordinated water O₂ by heating to transform into another single crystal with the formula of [Fe₃(NH₂-trz)₆(SCN)₅(H₂O)](SCN) (**2**).²⁸ Complex **2** can be reversed to **1** upon the reabsorption of water. Both complexes crystallize in the same orthorhombic chiral space group *P*2₁2₁2₁. Compared with the structures of **1** and **2**, they are very similar, except that the terminal coordinated H₂O molecule of Fe3 in **1** is replaced by a SCN[−] anion in **2** (Fig. 1a and b). It is of great interest that SCSC transformation in this case is involved with the breaking of the Fe–O bond (Fe3–O₂) and consequently the formation of a new Fe–N bond (Fe3–N29A) as illustrated in Fig. 1b, thus leading to the coordination environment of Fe3 changing from N₅O in **1** to N₆ in **2**. Careful inspection of the variation of Fe–N bond lengths of **1** and **2** from 293 to 100 K indicates that the origin of SCO phenomena is attributed to central Fe1 ion. Additionally, the transformation from **1** to **2** weakens N···H and O···H HBs. Thus, both trinuclear complexes exhibit a gradual SCO process but with different transition temperatures (*T*_{1/2} = 202 K for **1** and *T*_{1/2} = 160 K for **2**, Fig. 1c).

Structural dimensionality. Among the investigated SCO family, 1,2,4-triazole based Fe^{II} 1D coordination polymers are outstanding as characteristic of abrupt reversible spin transition and wide thermal hysteresis loops around room temperature.^{29,30} However, the long-standing challenge to

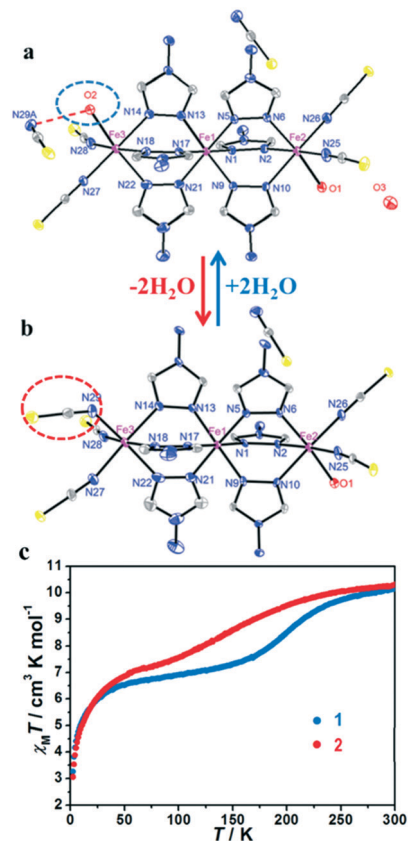


Fig. 1 Reversible desolvation between **1** (a) and **2** (b) and their corresponding temperature dependent magnetic susceptibilities (c). Adapted with permission from ref. 28.

Highlight

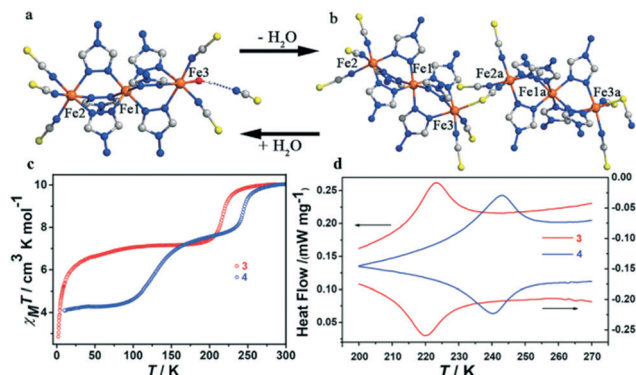


Fig. 2 SCSC transformation between **3** (a) and **4** (b), temperature-dependent magnetic susceptibilities (c) and DSC curves (d) for both complexes. Adapted with permission from ref. 32.

achieve single crystals of such 1D coordination polymers makes it difficult to probe and fine tune their high cooperativity.³¹ Moreover, SCSC transformation has the extraordinary capacity to construct variable and interesting structures, including the dimensionality changes from 0D to 2D, 1D to 3D and 2D to 3D.^{17,23} Recently a reversible SCSC transformation accompanied with change in dimensionality was observed between a linear trinuclear Fe^{II} complex [Fe₃(NH₂trz)₆(SCN)₅(H₂O)](SCN)·4H₂O (**3**) and a 1D chain [Fe₃(NH₂trz)₆(SCN)₅]_n(SCN)_n (**4**).³² An attempt to heat crystals of **3** at 130 °C for 30 min under a N_{2(g)} atmosphere led to dehydrated crystals of **4** with a colour change from pale yellow to yellow. The original crystals of **3** can be reversibly obtained by exposing **4** to water. In case of **4**, the trinuclear cluster is very similar to that of **3**, except that the terminal coordinated H₂O molecule (Fe3) is replaced by one of the SCN⁻ ligands of the neighbouring trinuclear cluster (Fig. 2a and b). Thus, the structure of **4** can be viewed as a 1D chain that consists of trinuclear clusters [Fe₃(NH₂trz)₆(SCN)₅]⁺, which are bridged by SCN⁻ anions. During the course of transformation, the coordination environment of Fe1 site shows negligible alternation and the variation of Fe–N bond lengths from 293 to 100 K (0.17 and 0.18 Å for **3** and **4**, respectively) is indicative of SCO behaviour. Unlike **3**, the average Fe2–N bond length of **4** decreases by about 0.18 Å from 293 to 100 K, suggesting that Fe2 ion also transforms

to LS at 100 K. Again no obvious Fe–N bond length change for Fe3 site can be observed. Deep insight into intra- and inter-molecular interactions reveals that HBs including O atoms are remarkably stronger. Therefore, the complicated 3D HB network derived from the clusters, lattice anions and lattice water molecules in **3** is stronger than that in **4**. SCO behaviours of both complexes are consequently modified from a one-step SCO characterized by $T_{1/2}^1 = 218$ K and $T_{1/2}^2 = 222$ K, with narrow hysteresis of 4 K corroborated by differential scanning calorimetry (DSC) curve in **3** to a two-step SCO (Fig. 2c and d) in **4**: one step centred at higher temperature ($T_{1/2} \sim 250$ K) is originating from the central Fe1 ion as **3**, and the lower step ($T_{1/2} \sim 125$ K) corresponds to the ligand field exerted on Fe2 ion. In this case, SCSC transformation not only increases the dimensionality of crystal structure, but also dramatically alters the SCO behaviour because of the small change in the coordination environments and intermolecular interactions.

Crystal symmetry. In some cases of ordered crystalline materials, SCSC process induced by solvent release makes a fascinating connection between SCO and structural phase transitions (SPTs).¹⁸ One possible character associated with SPTs in some cases can be mirrored by a crystallographic symmetry breaking upon formation of an intermediate phase.^{7,18,33–35} Neville *et al.* demonstrated a dynamic structural and SCO property interchange between solvated [Fe^{II}₂(*o*-Ntrz)₅(NCS)₄]₃MeOH (**5**·3MeOH) and desolvated products [Fe^{II}₂(*o*-Ntrz)₅(NCS)₄] (**5**, *o*-Ntrz = 4-(*o*-nitrobenzyl) imino-1,2,4-triazole) (Fig. 3).³⁶ Relatively uncommon, the guest molecules in **5**·3MeOH evolved *via* a SCSC transformation with affiliated phase transition ($P2_1/n \rightarrow C2/c$) resulting in two unique Fe^{II} sites observed for **5**·3MeOH which converts to a single crystallographical Fe^{II} site in **5** (Fig. 3) and the facile replacement of dinuclear...methanol interactions in **5**·3MeOH with new dinuclear...dinuclear interactions in **5**. A significant outcome of the increased symmetry in **5** is that one of the three $\mu_{1,2}$ -bridging ligands is centred over the C₂ axis, resulting in 2-fold disorder of the ligand, in which the peripheral NO₂ group is in two opposing positions in equal ratios (Fig. 3a and b). In consistency with the distinct structural difference, temperature-dependent magnetic susceptibility measurements reveal a broad

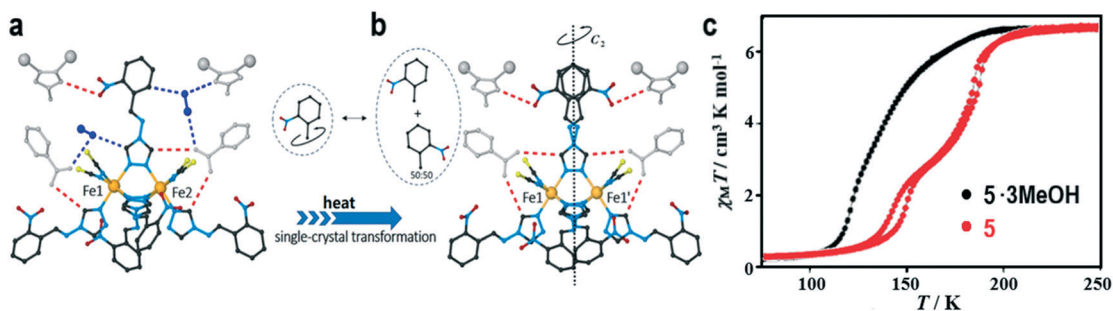


Fig. 3 SCSC transformation accompanied with the phase transition introducing a C₂ axis ($P2_1/n \rightarrow C2/c$) and dynamic ligand rotation between **5**·3MeOH (a) and **5** (b) as well as temperature-dependent magnetic susceptibilities for both complexes (c). Adapted with permission from ref. 36.

diversity of SCO profiles (Fig. 3c): 5·3MeOH displays a gradual, complete one-step SCO transition with a $T_{1/2}$ of 135 K while the complete, two-step SCO transition of **5** (2 K min^{-1}) is characterized by $T_{1/2}^{\downarrow} = 181$ K, $T_{1/2}^{\uparrow} = 185$ K, $T''_{1/2}^{\downarrow} = 141$ K and $T''_{1/2}^{\uparrow} = 148$ K, with narrow hysteresis widths ($\Delta T_1 = 4$ K, $\Delta T_2 = 7$ K). The reasoning for a two-step SCO is that the disposition of the NO_2 groups defines the short-range allocation of [HS–LS] or [LS–HS] spin-state assignment distribution.

This kind of solvent-induced symmetry breaking was also found in a mononuclear Co^{II} complex $[\text{Co}(\text{terpy})_2](\text{BF}_4)_2 \cdot \text{H}_2\text{O}$ (**6**· H_2O , terpy = 2,2':6',2''-terpyridine) (Fig. 4a). Complex **6**· H_2O can be transformed into $[\text{Co}(\text{terpy})_2](\text{BF}_4)_2$ (**6**) via a reversible SCSC process accompanied by a change from the tetragonal space group $I4_1/a$ to $P4_2/n$ but possessing similar crystal structures, intermolecular π – π and CH – π interactions. The major difference is that the BF_4^- anions in **6** are heavily disordered due to the absence of structural restriction by HBs compared with those present in **6**· H_2O (Fig. 4a). Interestingly, after dehydration the crystal packing structure maintained the crystal void observed in the unit cell of **6**· H_2O , reflecting the presence of strong lattice interactions present.³⁷ **6**· H_2O exhibits gradual and incomplete SCO, including the small stepwise changes of the $\chi_{\text{M}}T$ value found for **6**· H_2O , from fully HS to ca. 0.5 HS (Fig. 4b). This is attributed to the formation of HBs between water molecules and BF_4^- anions induced by the hydration process which clearly hinders such order/disorder transition for those anions. In contrast, the dehydrated phase **6** exhibits a reverse multistep hysteretic behaviour corresponding to the abrupt SCO in the low temperature region ($T''_{1/2}^{\downarrow} = 195$ K; $T''_{1/2}^{\uparrow} = 155$ K) and orbital (angular momentum) transition in the high temperature region ($T'_{1/2}^{\downarrow} = 287$ K; $T'_{1/2}^{\uparrow} = 270$ K) (Fig. 4b). Further temperature-dependent single-crystal X-ray structural analysis demonstrated that such a “cross loop” hysteresis, including the reverse and ordinary thermal hysteresis loops, can be ascribed to an order/disorder structural phase transition of BF_4^- anions involving a symmetry breaking to yield the monoclinic space group $P2_1/n$ and orbital transition.

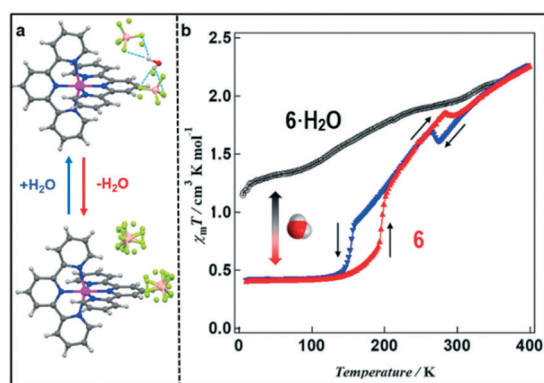


Fig. 4 Single-crystal structures (including disordered BF_4^- anions) (a) and temperature-dependent magnetic susceptibilities for **6** and **6**· H_2O (b). Adapted with permission from ref. 37.

Nevertheless, symmetry breaking is not a requirement to observe such phenomenon. Indeed, in case of complex $[\text{Fe}^{\text{II}}(\text{H}_4\text{L1})(2\text{bbp})][(\text{ClO}_4)_2 \cdot 3\text{C}_3\text{H}_6\text{O}]$ ($7 \cdot 3\text{C}_3\text{H}_6\text{O}$; $\text{H}_4\text{L1} = 2,6$ -bis-(5-(2-methoxyphenyl)-pyrazol-3-yl)-pyridine; $2\text{bbp} = 2,6$ -bis(pyrazol-3-yl)pyridine), the solvent extrusion proceeding via a SCSC process with persistence of crystal symmetry ($P\bar{1}$) is accompanied by a spin state switch, from HS to LS.³⁸

Cis-to-trans isomerization. An unprecedented solvent-release induced supramolecular isomerization in the 2D Fe^{II} SCO system with a dramatic structural transformation from *cis*- $[\text{Fe}^{\text{II}}(2,4\text{-bpt})_2] \cdot 4\text{H}_2\text{O}$ (**8**· $4\text{H}_2\text{O}$) to *trans*- $[\text{Fe}^{\text{II}}(2,4\text{-bpt})_2]$ (**8**), where 2,4-Hbpt = 3-(2-pyridyl)-5-(4-pyridyl)-1,2,4-triazole, was reported by Tong *et al.* (Fig. 5).³⁹ During the solvent-release transformation, three major structural changes occur: (a) the coordination configurations of 2,4-bpt ligands to the metal ions are transformed from *cis* in **8**· $4\text{H}_2\text{O}$ to *trans* in **8** as concluded from a DSC analysis with an endothermic peak centred at ~ 610 K followed by an exothermic peak centred at ~ 615 K (Fig. 5b), resulting in 2D (4,4) wavy (in **8**· $4\text{H}_2\text{O}$) and planar (in **8**) layers, respectively; (b) the crystal packing are transformed from a microporous structure with 1D channels in **8**· $4\text{H}_2\text{O}$ to a nonporous close packing structure in **8** (Fig. 5a); (c) compared to hydrated complex, dehydrated complex **8** shows an increase of the ligand-field strength as well as an enhancement of the cooperativity. The shrinkage of average Fe–N bond length from **8**· $4\text{H}_2\text{O}$ ($d_{\text{Fe-N}} = 2.08$ Å) to **8** ($d_{\text{Fe-N}} = 2.0$ Å) provides direct proof for the enhancement of ligand-field strength. Moreover, no evident interframework HBs in **8**· $4\text{H}_2\text{O}$ may be responsible for the less cooperative nature and more gradual SCO curve. As a result, the SCO nature is altered from a gradual incomplete type (**8**· $4\text{H}_2\text{O}$) to an abrupt and complete type ($T_{1/2}^{\downarrow} = 269.7$ K and $T_{1/2}^{\uparrow} = 268.4$ K, **8**) (Fig. 5c)

Supramolecular interaction. As mentioned above, solvent molecules in the crystal lattice play a very important role in tuning the transition temperature. Also, a solvent responsive effect based on single crystal structures is a convenient and significant tool for probing the SCO phenomena in the solid state. In essence, solvent molecule usually participates in rich HB interaction between the lattice solvent and coordination ligands, thus forming a rigid environment of complex cations and generating the possible internal pressure to lock the spin state in the LS one. In contrast, removal of lattice solvent molecules unlocks those HB interactions, prone to destabilize the LS state.^{18,34,40–43} Moreover, in some cases, solvent-free materials feature intrinsic abrupt and thermal hysteresis SCO at lower temperatures due to orientational ordering of anions and π – π stacking of coordination ligands.⁴²

Taking advantage of such on–off SCO behaviour induced by solvent-release SCSC process, SCO-active materials represent an important promise as solvent sensor. In this regard, two reversible quantitative solvent sensors by SCO-active materials were reported in two mononuclear Fe^{II} complexes, $[\text{Fe}^{\text{II}}(\text{tolpzph})_2(\text{NCS})_2] \cdot \text{THF}$ (**9**·THF, $\text{tolpzph} = 4$ -*p*-tolyl-3-(phenyl)-5-(2-pyrazinyl)-1,2,4-triazole)⁴⁴ and $[\text{Fe}(\text{aqin})_3](\text{BPh}_4)_2 \cdot 2\text{CH}_3\text{CN}$ (**10**· $2\text{CH}_3\text{CN}$, where $\text{aqin} = 8$ -aminoquinoline).⁴⁵ Of particular

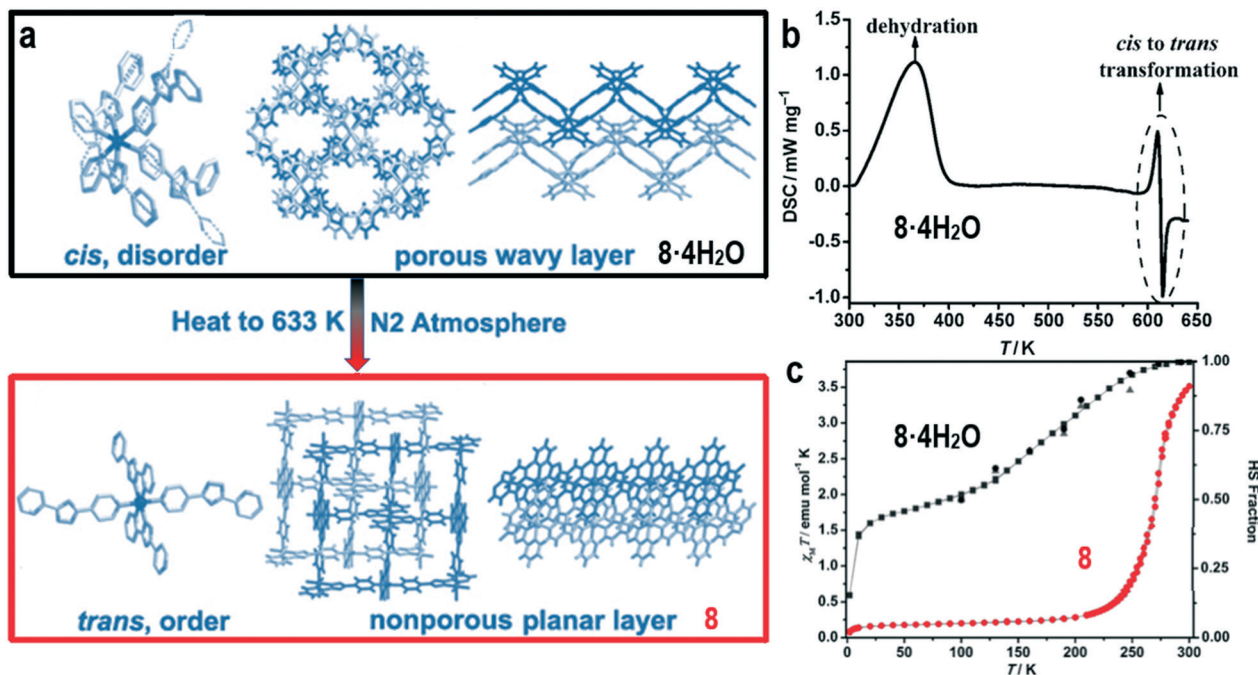


Fig. 5 SCSC transformation between $8 \cdot 4\text{H}_2\text{O}$ and **8** (a), DSC curves for $8 \cdot 4\text{H}_2\text{O}$ (b) and temperature-dependent magnetic susceptibilities for both complexes (c). Adapted with permission from ref. 39.

interest is that they exhibit a highly sensitive solvent-release dependent occurrence of SCO and $T_{1/2}$ was found to be linearly dependent on the mole fraction of the solvent molecule present. The observed shift in $T_{1/2}$ as the solvent concentration is decreased, is likely to be due to internal lattice pressure effects. Furthermore, for complex $10 \cdot 2\text{CH}_3\text{CN}$, SCSC transformation occurred to give solvent-free phase **10** with the dramatic change of HB interaction involved with a CH_3CN molecule. In $10 \cdot 2\text{CH}_3\text{CN}$, one of the solvated CH_3CN molecules participates in the formation of two type HBs: one involves the $-\text{NH}_2$ groups of aqin and the other involves the phenyl ring of BPh_4^- ions. Moreover, the CH_3CN molecule is involved in abundant short contacts and relatively stronger edge-to-face $\text{C}-\text{H} \cdots \pi$ interactions. Presumably, it is such combination of HB interactions which leads to the slow and successive release of solvent molecules in the repeated heating and cooling magnetic measurement.

Another successive and reversible SCSC transformation occurred in following complexes, $[\text{Fe}^{\text{II}}(\text{L}2)_2(\text{NCS})_2] \cdot 3\text{MeOH}$ (**11**·3MeOH) = $[\text{Fe}^{\text{II}}(\text{L}2)_2(\text{NCS})_2]$ (**11**) = $[\text{Fe}^{\text{II}}(\text{L}2)_2(\text{NCS})_2] \cdot 2\text{H}_2\text{O}$ (**11**·2H₂O) (L2 = 2-(anthracen-10-yl)-1H-imidazo[4,5-f][1,10]phenanthroline), simply by solvent desorption–resorption.⁴⁶ These solvent-release SCSC transformations feature the reversible trimming of intermolecular solvent \cdots imidazole \cdots solvent HBs in **11**·Solv, which results in SCO on–off switching.

In contrast to the overwhelming majority of $\text{Fe}^{\text{II/III}}$ -based SCO complexes immersed in the “magic” N_6 or N_4O_2 coordination sphere,⁶ Co^{II} SCO complexes are restricted to terpyridine-like (terpy), imine-based and macrocyclic ligands.⁴⁷ Commonly, the spin conversion in Co^{II} complexes is gradual, incomplete and without hysteresis.^{48–50} To explore the potential

of Co^{II} complexes for the switchable bistability, Wang *et al.* demonstrated an unprecedented on–off switching of SCO behaviours triggered by a reversible SCSC transformation during dehydration–rehydration of two Co^{II} complexes, $[\text{Co}^{\text{II}}(\text{L}3)_2](\text{DPAS})_2 \cdot \text{DMF} \cdot 2\text{H}_2\text{O}$ (**12**·2H₂O), and its dehydrated form $[\text{Co}^{\text{II}}(\text{L}3)_2](\text{DPAS})_2 \cdot \text{DMF}$ (**12**, L3 = 4’-(4-bromophenyl)-2,2’:6’,2’’-terpyridine and $\text{DPAS}^- = 4$ -(phenylamino)benzene-sulfonate) (Fig. 6).⁵¹ The dehydration process occurred in a SCSC fashion when the dark red crystals of **12**·2H₂O were heated under a dry nitrogen gas flow on the X-ray diffractometer. Interestingly, upon exposure to air for one day, dehydrated crystals can reversibly return to the hydrated ones. Both complexes crystallized in the triclinic space group *P1* with similar structures, except for the loss of two H₂O molecules in **12** (Fig. 6a). Variable temperature magnetic susceptibilities of both cases confirmed the different thermal behaviours (Fig. 6c). For **12**·2H₂O, the cooling and heating temperature-dependent thermal behaviours display the same profile with a complete SCO from $S = 3/2$ to $1/2$ with $T_{1/2}$ of 125 K, while the typical pure HS anisotropic spin centre of $S = 3/2$ exits at all temperatures without no spin state change in **12**. A careful inspection of the supramolecular interactions was taken in consideration hereafter. In **12**·2H₂O, the DPAS^- anions and water molecules form 1D ladders along *a* axis connected by $\text{N}-\text{H} \cdots \text{O}$ and $\text{O}-\text{H} \cdots \text{O}$ HBs. Interestingly, half of the L3 ligands (L_A) are locked inside the square windows of the ladders by $\text{C}-\text{H} \cdots \text{O}$ HBs between the O atoms from H₂O, the SO_3^- and $\text{C}-\text{H}$ groups from L_A ligands. Besides there are also $\pi-\pi$ interactions between the pyridine rings of L_B and the benzene rings of the DPAS^- anions (Fig. 6b). After SCSC dehydration, HBs involving H₂O molecules are all removed accompanied with the disappearance of HBs

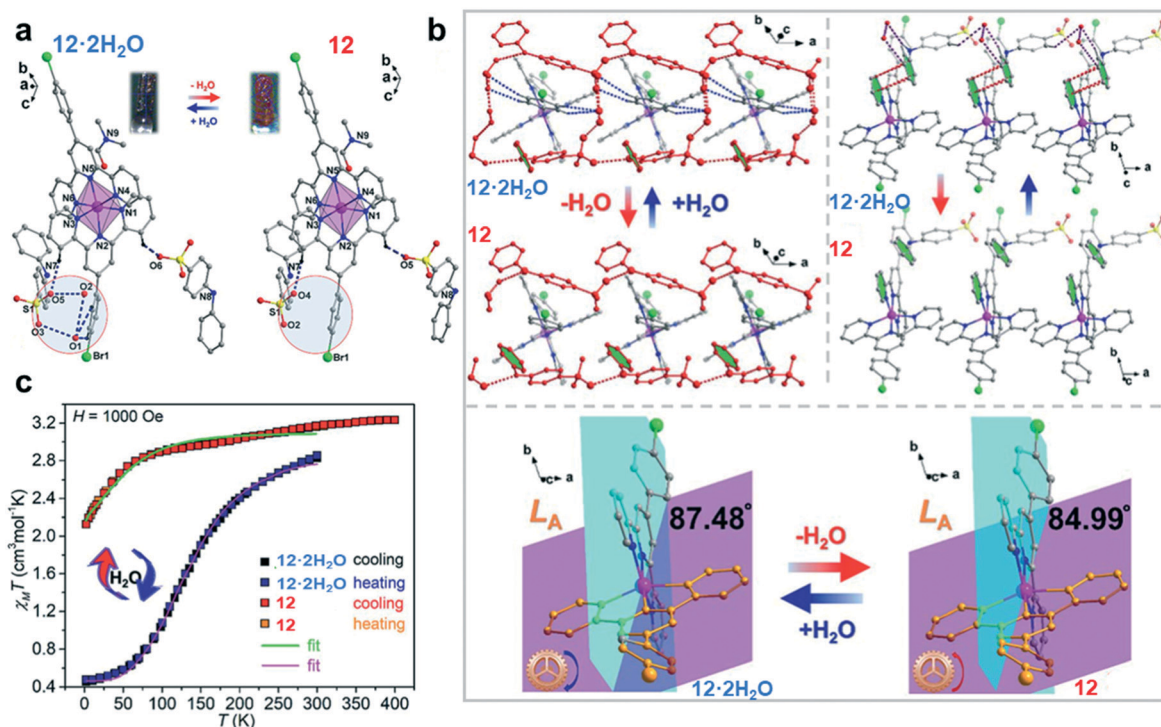


Fig. 6 Structure (a and b) and magnetic properties via SCSC transformation for 12·2H₂O and 12 (c). Adapted with permission from ref. 51.

ladders and the locking effect of the L_A ligands; as well as the weakness of the π - π interactions mentioned above due to the rotation of the benzene rings of the DAPS⁻ anions. Consequently, the L3 ligands in **12** are much more loosely packed compared to those in 12·2H₂O, which results in a more distorted octahedron of the Co^{II} center in **12** confirmed by the larger continuous shape measured values (4.365 for 12·2H₂O vs. 4.653 for **12** at 300 K) as well as by the larger distortion parameters Σ and θ ($\Sigma = 90.4^\circ$ and $\theta = 305^\circ$ for 12·2H₂O vs. $\Sigma = 91.7^\circ$ and $\theta = 316^\circ$ for **12** at 300 K) (Σ is the sum of the deviation from 90° of the 12 *cis* angles of the CoN₆ octahedron; θ is the sum of the 24 unique N-Co-N angles measured on the projection of two triangular faces of the octahedron along their common pseudo-3-fold axis) and the smaller dihedral angle between the least-square planes of the two L3 ligands (87.48° in 12·2H₂O vs. 84.99° in **12** at 300 K, Fig. 6b). Apparently, the large distortion of the Co^{II} octahedron stabilizes the HS state in **12**. Such solvent-release SCSC transformation induces significant geometrical changes of the Co^{II} centre and modification of the supramolecular interactions, then switches its colour and magnetic properties.

Successive efforts were devoted to the modification of the anions to further develop dynamic molecular Co^{II} complexes, replacing the flexible DPAS⁻ with rigid BDS²⁻ which bears more potential of HBs. This way, two novel Co^{II} complexes, [Co^{II}(L3)₂][BDS]·2H₂O (**13**·2H₂O) and [Co^{II}(L3)₂][BDS] (**13**, H₂BDS = benzene-1,3-disulfonic acid) were obtained, whose hysteretic SCO can be reversibly switched on and off through a dehydrated-hydrated SCSC fashion.⁵² Although both complexes have similar single crystal structures, careful

examination of the intermolecular interactions in both 13·2H₂O and **13** revealed the structure–function relationship of the switchable SCO properties upon dehydration. By consideration of HBs aspect, in 13·2H₂O, two BDS²⁻ anions are linked together by four H₂O molecules connected by OH \cdots O HBs. These strong HBs in 13·2H₂O form a rigid environment of the complex cations and generate the possible internal pressure to prevent the expansion of the Co^{II} coordination sphere, thus locking the spin state of 13·2H₂O in the LS state, and then hindering its spin state switching. Removal of lattice water unlocked those strong HB interactions in **13** leading to a decrease in the internal pressure and stabilizes the HS state. By considering of π \cdots π interactions, the dehydrated process leads to significant shortening of the π \cdots π distances (3.438–3.651 Å) compared to 13·2H₂O (3.459–3.771 Å), which could be favourable for a cooperative spin transition. A pronounced decrease of N1–Co–N5 bond angle from 112.05 to 100.63° relative to the spin transition from HS to LS in **13**, is responsible for the anisotropic expansion and contraction of the lattice. Consequently, the hysteretic SCO ($T_{1/2}^{\uparrow} = 267$ K and $T_{1/2}^{\downarrow} = 235$ K) in the dehydrated complex **13** is ascribed to the combination of guest internal pressure loss, the supramolecular interactions change, and the strong electron–lattice coupling.

2.2. Solvent-exchange SCSC transformations

Materials capable of sensing volatile guests *via* a SCSC transformation triggered by migration of small molecules

Highlight

through a lattice (absorption, desorption or exchange) are of great appeal for development as chemical sensors using spin switching to signal detection.^{21,53,54} Recent developments in this field have manifested SCO frameworks as one type interesting candidates for potential sensing applications.^{3,8,55–57} Considerable efforts have also been made to explore the solvent influence on SCO behaviour in molecular materials. The guest exchange occurs in molecular materials by diffusion through the crystal lattice accompanied with the conformational reorganization to accommodate the guest molecule.^{54,58} Hence careful design is required in order to access robust and flexible molecular systems that facilitate the diffusion of gaseous guest species maintaining its single crystallinity during uptake = release recycle.⁵³ Noticeable examples include [Fe(tpa)(NCS)₂] (**14**, tpa = tri(2-pyridylmethyl)amine)^{7,59} and [Fe(liq)₂](BF₄)₂·Et₂O (**15**·Et₂O, liq = 3-((1*H*-imidazol-4-yl)methyleneamino)-2,3-dihydro-2-(1*H*-imidazol-4-yl)quinazolin-4(1*H*)-one),⁶⁰ both showing vapochromic, distinct structural and SCO behaviour transformations with solvent modulations. Exposure of single crystals of **14** to methanol vapor caused a dramatic yellow-to-red colour change and subsequent crystallographic studies established the structure of a new complex, formulated as {[Fe(tpa)(NCS)₂]₂·[Fe(tpa)(NCS)₂·CH₃OH]} (**14**-MeOH), whose asymmetric unit contains two crystallographically independent molecules of Fe(tpa)(NCS)₂, one of which featuring strong HB interaction with a methanol molecule. Magnetic measurements revealed a one-step, incomplete SCO of **14** while the studies of **14**-MeOH showed a two-step process ($T'_{1/2} = 229$ K and $T''_{1/2} = 303$ K).⁷ The SCSC transformation from **15**·Et₂O to **15**·3H₂O occurred upon humidity exposure and reversible recovery of its crystallinity upon exposure to ether vapor. The etherified phase **15**·Et₂O exhibits room temperature SCO ($T_{1/2} = 305$ K) but negligible thermal hysteresis while the hydrated phase **15**·3H₂O exhibits an apparent hysteresis loop ($T_{1/2}^{\uparrow} = 346$ K, $T_{1/2}^{\downarrow} = 326$ K).⁶⁰

Another example includes substantial adaptability of nonporous complex to structural transformations, on the basis of an azole-type ligand. This way, a robust non-porous SCO-active dinuclear Fe^{II} complex, [Fe₂(L4)₂(MeCN)₄](BF₄)₄·2MeCN (**16**·2MeCN, L4 = 4-(4-methylphenyl)-3-(3-pyridazinyl)-5-pyridyl-4*H*-1,2,4-triazole) has been reported to undergo a reversible SCSC transformations on exposure to a variety of solvent vapours, MeCN = EtOH → H₂O = MeCN, with the associated colour changes and magnetic response providing easy readout of the identity of the bound guest.⁵³

Garcia *et al.* discussed the capacity of the neutral Fe^{II} molecular material [Fe(trz-tet)₂(H₂O)₄].4H₂O (**17**, trz-tetH = 5-(4*H*-1,2,4-triazol-yl)-2*H*-tetrazole) as a colorimetric sensor for a wide spectrum of vapor-phase analytes (MeOH, EtOH) including toxic gases (HCl, HBr, hydrazine monohydrate, ammonia) (Fig. 7a).^{61–63} ⁵⁷Fe Mössbauer spectroscopy was applied to investigate the driving spin state change of the analytes in this Fe-azole sensor material (Fig. 7b). In particular, the pink colour detection (*e.g.*, obtained with MeOH(g)) was systematically associated to the emergence of Fe^{II}N₆ LS ions as shown by diffuse reflectance spectroscopy.

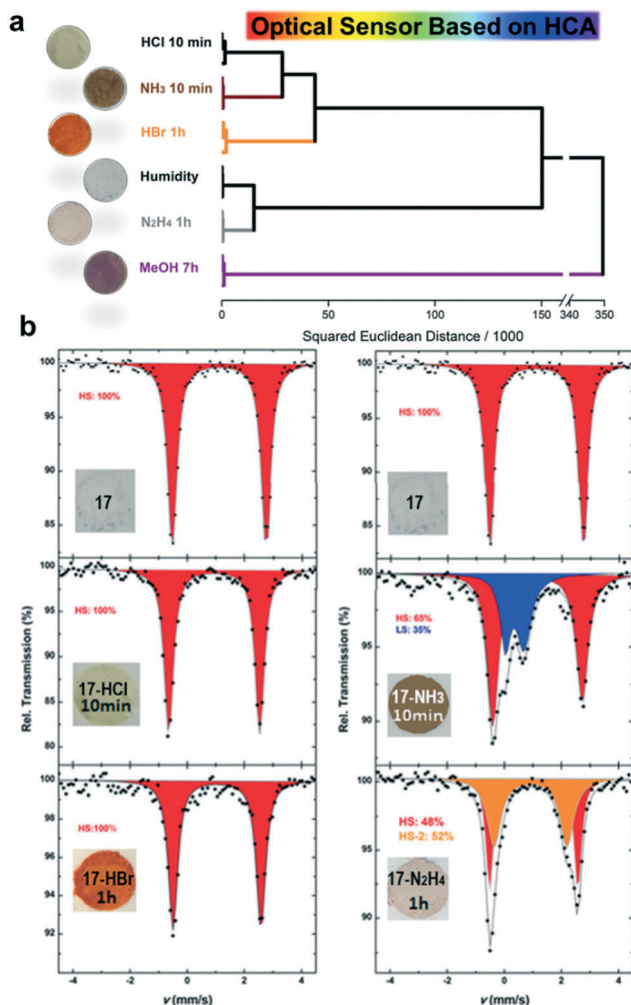


Fig. 7 HCA dendrogram with Ward linkage for 4 TICs, MeOH and one humidity test at full vapor pressure of **17** at room temperature (a) and Mössbauer spectra prepared at 300 K (b). Adapted with permission from ref. 62.

Clear colour differentiation among four different toxic industrial chemicals (TICs) and alcohols was demonstrated (Fig. 7a). Different TICs and alcohols were readily identified using a standard chemometric approach (hierarchical clustering analysis), with no misclassifications over 18 trials (Fig. 7a).

Another best candidate to investigate SCO behaviour triggered *via* a guest-exchange induced SCSC transformation is tris-imine related Fe^{II} complexes.^{12,34,38,54,57,58,64,65} This lies in the fact that most of those kind molecules with a dense network of intermolecular interactions not only have the flexible ability to facilitate the diffusion of small molecules through the lattice but also maintain the integrity of the crystallographic order and single crystallinity.⁵⁴ In particular, Aromi's group designed and synthesized a novel bpp-based ligand, H₂L5 (H₂L5 = 2,6-bis(5-(2-methoxyphenyl)pyrazol-3-yl)pyridine), and while combining it to bpp (bpp = 2,6-bis(pyrazol-3-yl)pyridine), they managed to produce one type of heteroleptic coordination complex [Fe(bpp)(H₂L5)]

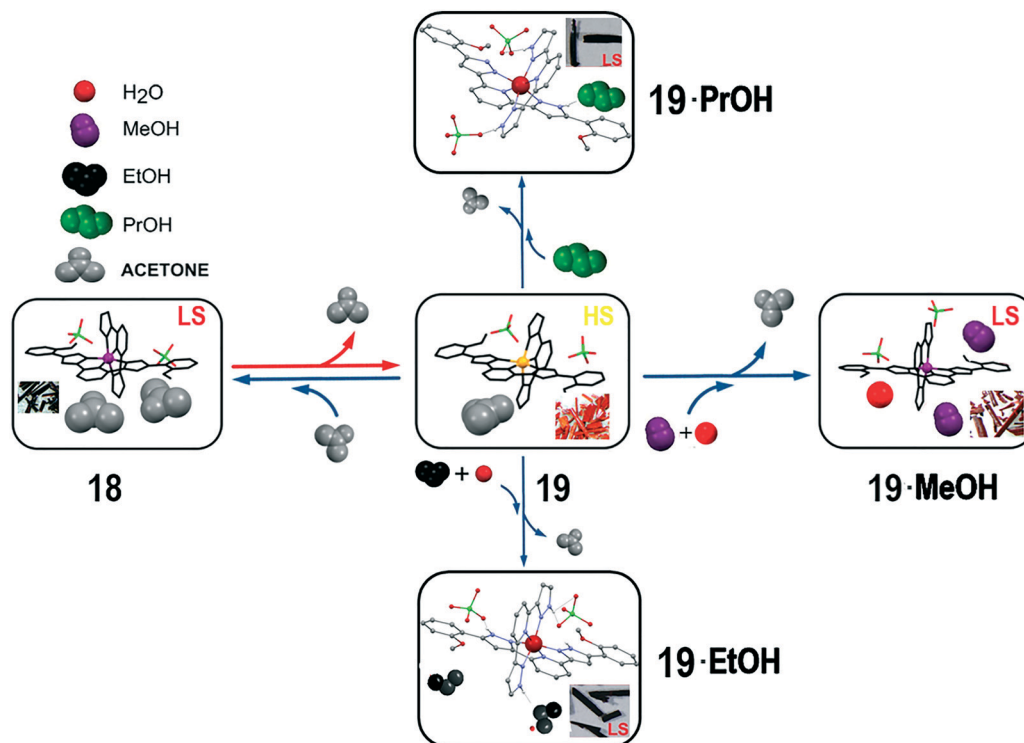


Fig. 8 Representation of the molecular structure emphasizing the full SCSC transformation undergone by these five species through subsequent absorption, desorption, or exchange of small molecules. Adapted with permission from ref. 54 and 58.

$(\text{ClO}_4)_2 \cdot 1.5\text{acetone}$ (**18**) with the ability to extrude one-third of acetone molecules to lead to $[\text{Fe}(\text{bpp})(\text{H}_2\text{L5})](\text{ClO}_4)_2 \cdot \text{acetone}$ (**19**) upon heating, while switching to the HS state and experiencing a profound crystallographic change with the symmetry change from $P2_1/n$ to $P\bar{1}$.^{58,66} Other remarkable transformations in **19** are the simultaneous rotation by $\sim 180^\circ$ of both methoxyphenyl groups of $\text{H}_2\text{L5}$ in every other cation together with a change of the average Fe–N bond distances to 2.169 Å, indicative of Fe^{II} centres in the HS state. Of particular interest is that the remaining acetone molecules in **19** could be replaced by MeOH, EtOH and *n*-PrOH, to form a series of new complexes with the formula of $[\text{Fe}(\text{bpp})(\text{H}_2\text{L5})](\text{ClO}_4)_2 \cdot 1.25\text{MeOH} \cdot 0.5\text{H}_2\text{O}$ (**19**·MeOH), $[\text{Fe}(\text{bpp})(\text{H}_2\text{L5})](\text{ClO}_4)_2 \cdot 1.5\text{EtOH} \cdot 0.5\text{H}_2\text{O}$ (**19**·EtOH) and $[\text{Fe}(\text{bpp})(\text{H}_2\text{L5})](\text{ClO}_4)_2 \cdot \text{PrOH}$ (**19**·PrOH), respectively.⁵⁴ For all those transformations, a drastic colour change takes place from orange/yellow to very dark red (Fig. 8), which can serve as a mechanism for detecting the absorption of any of the three alcohols from the atmosphere around crystals of **19**. The nature of the alcohol absorbed can be detected by the signature of the thermal magnetic behaviour of the resulting material. In all cases, a HS-to-LS spin state switching occurs with the solvent exchange, and the $\chi_M T$ products obtained become HS again on increasing the temperature as a result of the combination of SCO and solvent extrusion processes, in each case with a different characteristic transition temperature.

Harding and McMurtrie reported an anionic supramolecular framework-like adduct $[\text{Fe}^{\text{III}}(\text{qsal-OMe})_2][(\text{IFB})$

(NCS)] (**20**) with potential magnetic sensing through a reversible exchange of MeOH and H_2O , where $\text{qsal-OMe} = 5\text{-methoxy-8-quinolylsalicylaldimine}$ and $\text{IFB} = 1,3,5\text{-triodotrifluorobenzene}$.⁶⁷ The repeated and reversible SCSC transformation occurs within complexes $[\text{Fe}^{\text{III}}(\text{qsal-OMe})_2][(\text{IFB})(\text{NCS})] \cdot \text{MeOH}$ (**20**·MeOH) and $[\text{Fe}^{\text{III}}(\text{qsal-OMe})_2][(\text{IFB})(\text{NCS})] \cdot \text{H}_2\text{O}$ (**20**· H_2O), via a desolvate (–MeOH), hydrate (+ H_2O), dehydrate (– H_2O), and resolvate (+MeOH) recycle associated with the dramatic change of structure and spin transition

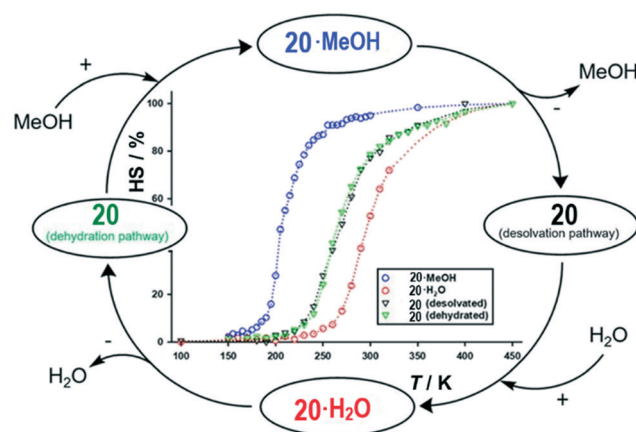


Fig. 9 VT-SCXRD magnetic profile and reversible solvation and hydration cycle of **20** (black and green traces), producing **20**·MeOH (blue trace) and **20**· H_2O (red trace) through the absorption of methanol or water. Adapted with permission from ref. 67.

(Fig. 9). The crystal structures of three complexes at 180 K show similar crystal packing, the most significant differences lie in supramolecular interaction. The $\text{NCS}^- \cdots \text{solvent} \cdots 1,3,5\text{-IFB} \cdots \text{NCS}^- \cdots \text{solvent}$ six-component $2 + 2 + 2$ mixed HB/XB motif observed in **20-Solv** is replaced by a four-component $2 + 2$ XB motif involving $\text{I} \cdots \text{NCS}^- \cdots \text{I}$ ($1,3,5\text{-IFB} \cdots \text{NCS}^- \cdots 1,3,5\text{-IFB}$) contacts. Also the XB units in the crystal structure imbue sufficient stability to **20** for it to repeatedly and reversibly desolvation–solvation SCSC transformation with negligible loss of crystalline integrity. The result is a reversible solvatomorphic hysteresis between the methanolate and hydrate with $\Delta T_{1/2} = 95$ K. Furthermore, at 260 K (50:50 LS/HS population), crystal of **20** represents a tristable spin system that can be switched into either LS or HS by exposure to H_2O or MeOH. Therefore, selective magnetic sensors based on crystalline **20** could be used to identify MeOH or H_2O in the presence of a wide variety of other solvents or molecules.

Recently, Tong's group developed a molecular crystal $[\{\text{Fe}^{\text{III}}(\text{salten})\}_2(\text{TPB})](\text{BPh}_4)_2$, where $\text{H}_2\text{salten} = N,N'$ -bis(2-hydroxyphenyl) methylene-4-azaheptane-1,7-diamine, TPB = 1,2,4,5-tetra(4-pyridyl) benzene (**21**, hereafter named as phase **21-I**) by associating the rotatable tetraphenylborate anion with Fe^{III}_2 SCO cation (Fig. 10a).⁶⁸ The solvent-free phase **21-I** can undergo a temperature-induced phase transformation to phase

21-II with the same molecular components but with distinct conformational changes of the salten^{2-} ligand due to the rotation of the BPh_4^- anion, giving rise to fascinating variations in SCO from gradual to abrupt. Structural transformations between different spin states are more prominent in **21-II** revealed by the larger variation of the average Fe–O/Fe–N bond length compared to **21-I**. In particular, such thermal-driven transformations make the four phenyl rings of the BPh_4^- anion experience different degrees of rotation, with the largest rotation occurs in the C34–C39 phenyl ring with a rotation angle change from 36.72° in **21-I** to 89.58° in **21-II**, therefore resulting in a thoroughgoing change in the surrounding intermolecular interactions (Fig. 10b). Consequently, more robust phenyl rotations of the BPh_4^- anion and striking variations of Fe^{III} geometry are achieved between LS and HS states, leading to an abrupt spin transition in **21-II**. Most importantly, **21-II** phases occur a reversible solvent-vapor and temperature-induced SCSC polymorphic transformations to form solvent-free phases **21-III** and **21-IV**, which could be applicable as solvent sensors. **21-III** and **21-IV** display larger thermal hysteresis loops up to 15 and 11 K, respectively. The $T_{1/2}$ values of **21-III** and **21-IV** move down to 221 and 225 K, while the warming dynamics are unchanged (Fig. 10c). In addition, **21-III** and **21-IV** can convert to **21-II** by annealing at 380 K for 2 h. Although similar in molecular structure and packing to **21-II**, subtle differences in **21-III** and **21-IV** were revealed by carefully checking the rotational movements of the BPh_4^- anions, which are slightly larger than those in **21-II**. Surprisingly, the solvent-vapor induced polymorphic transformation from **21-II** to **21-III** or **21-IV** is not involved with lattice solvent exchange, the mechanism may be induced by interfacial HB interactions between polar solvents and external molecules, which then trigger a cascade of the subtle structural rearrangement throughout the whole crystal.

3. Light-induced SCSC transformations

Complexes grafted with photoresponsive ligand moieties can induce spin state transition upon light-induced conformational changes and are thus considered as a new class of photoswitchable SCO materials.⁶⁹ In essence, SCO is triggered at the coordinated metal ion remotely *via* photochemical reaction at the photoisomerizable ligand. Several well-known photochromic building units have been introduced into SCO systems to develop novel photoresponsive magnetic materials,^{69,70} involving the *cis-trans* photoisomerization of stilbenes^{71–73} or azobenzenes,⁷⁴ the intramolecular photocyclization of dithienylethene^{75–81} as well as the photochemical $[2 + 2]$ cycloaddition reaction.⁸² In this section, we shall focus on the last two types.

3.1. Structural transformations *via* photoinduced cyclization

Diarylethene photochromes represent attractive molecules due to their remarkable properties which includes their: a) extensively chemical functionalization, b) reversible bi-

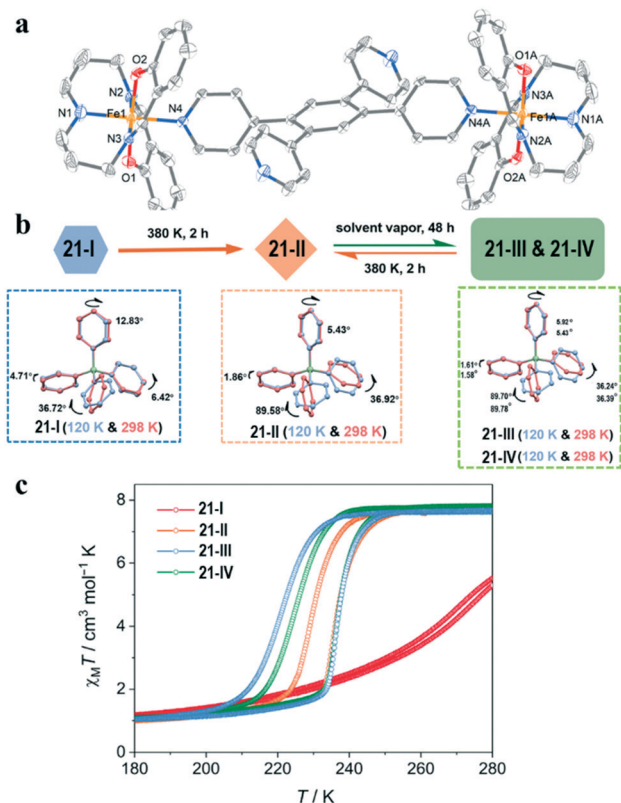


Fig. 10 The structure of $[\{\text{Fe}^{\text{III}}(\text{salten})\}_2(\text{TPB})]^{2+}$ (a), the schematic SCSC transformation pathways and the rotational movements of the BPh_4^- anion for **21-I**, **21-II**, **21-III** and **21-IV** (b) and variable-temperature magnetization of the four polymorphs with a sweep rate of 2 K min^{-1} (c). Adapted with permission from ref. 68.

directional light switching, following a closing/opening of a carbon atoms ring, c) thermal stability for the open and closed isomers and d) excellent fatigue resilience and fast photochromic responsiveness. As a result, the incorporation of diarylethene ligands into spin-active species renders the possibility to obtain photochromic materials and at best photomagnetic ones.⁷⁵ Despite significant progress in photoswitching through ligand-driven effects in the liquid phase,^{75,79,81} only a few attempts to observe the unidirectional^{76,78} or reversible photoswitching^{77,80} in the solid state, as required for applications, have been successful.

The first type of Fe^{II} complexes, [Fe(L6)₄(NCS)₂] (22)⁸³ and [Fe(L7)₂(NCS)₂·2MeOH] (23)⁸⁴ (where L6 = 4-[4-[3,3,4,4,5,5-hexafluoro-2-(2-methyl-5-phenylthiophen-3-yl)-cyclopent-1-enyl]-5-methylthiophen-2-yl]pyridine, L7 = 1,2-bis(2'-methyl-5'-(pyrid-4'-yl)thien-3'-yl)perfluorocyclopentene) show merely reversible photochromic transformation in the solid state rather than the desired photoswitchable SCO *via* ligand photoisomerization, although room temperature photomagnetism was observed for 23, presumably through an electron transfer mechanism.⁸⁴

By introducing a photoactive diarylethene-based ligand, phen* to the SCO iron(II) complex, [Fe(H₂B(pz)₂phen*)] (24, pz = 1-pyrazolyl, phen* = 5,6-bis(2,5-dimethyl-3-thienyl)-1,10-phenanthroline), magnetic properties in the solid state have been varied *via* ligand photoisomerization. In particular, the alternating irradiation with UV and visible light induces reversible isomerization of the photoactive ligand, which in turn triggers reversible SCO at the coordinated magnetic centre.⁷⁷

A novel bis(pyrazolylpyridyl) ligand, 1,2-bis(5-(2-(pyrazol-3-yl)pyridin-5-yl)-2-methyl-thiophen-3-yl)-cyclopentene (L8), featuring a central photochromic dithienylethene spacer assembled with

Fe^{II} to construct a molecular triple stranded helicate [Fe₂(L8)₃]⁴⁺ (25), was recently reported.⁷⁸ The configuration of the methyl groups in the dithienylethene units is antiparallel with their carrier carbon atoms within each unit separated by <4 Å, which fulfils the structural requirement to expect the photocyclization. Irradiation of crystals of 25 with UV light ($\lambda < 425$ nm) led immediately to a colour change from orange to dark brown. However, the reverse process was not observed even after long exposure to visible light possibly ascribed to the accommodation within the lattice of modifications (C-H... π and solvent...ClO₄⁻ intra- or intermolecular interactions) associated with the ring closure to prevent the structural changes necessary for reopening the cycle. Consistent with the above-described colour changes upon irradiation, the unidirectional transformation from open to closed occurs. *Ex situ* irradiation of 25 with UV light at room-temperature produces a sizable change to the magnetic response of the material that is not reversible.

Based on a new photochromic bis(bipyridine)-substituted diarylethene ligand, 1,2-bis(5-([2,2'-bipyridin]-5-yl)-2-methylthiophen-3-yl)cyclopentene (L9), three self-assembled Fe^{II} complexes, [Fe^{II}₂(*o*-(L9)_{anti})₃](OTf)₄ (26), {Fe^{II}₂(*o*-(L9)_{syn})₂}[Fe^{III}(Tp*)(CN)₃]₂}[Fe^{III}(Tp*)(CN)₃]₂·H₂O·3CH₃CN (27, Tp* = hydro-tris(3,5-dimethylpyrazol-1-yl)borate), [Fe^{II}₂(*c*-(L9))₃](OTf)₄·5.5 H₂O (28), that comprised an anti-parallel open form (*o*-(L9)_{anti}), a parallel open form (*o*-(L9)_{syn}), and a closed form (*c*-(L9)) of diarylethene conformers, respectively, were isolated (Fig. 11).⁸⁰ Fe^{II}₂(*o*-(L9)_{anti})₃ is a dinuclear structure where the two Fe^{II} centres are coordinated and bridged using three L9 ligands with an anti-parallel conformation. Both Fe^{II} centres are characterised by an N₆ coordination environment with an average Fe–N distance of

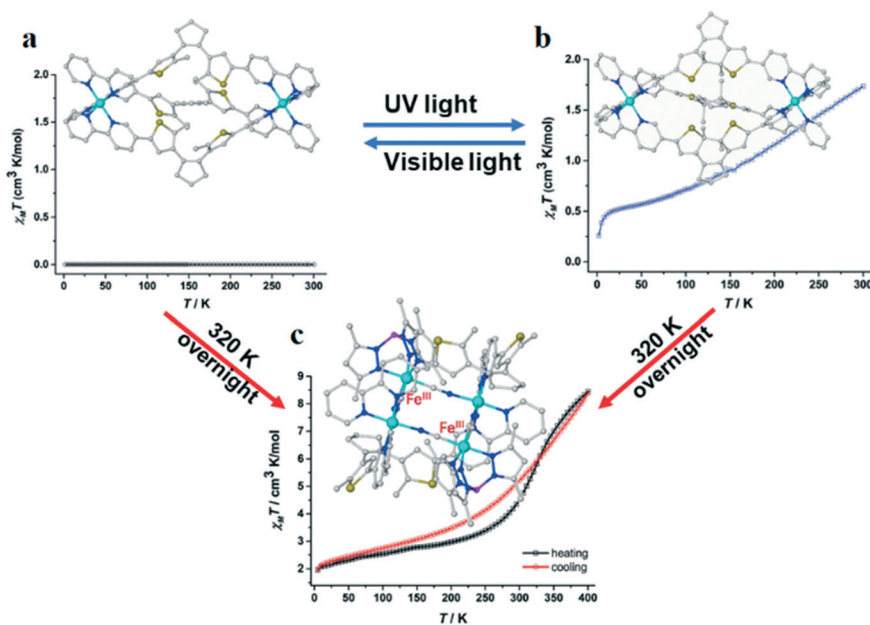


Fig. 11 Single-crystal structure and magnetic properties of Fe^{II}₂(*o*-(L9)_{anti})₃ (a), calculated structure and magnetic properties of Fe^{II}₂(*c*-(L9))₃ (b), as well as single-crystal structure and magnetic properties of Fe^{III}₂Fe^{II}₂(*o*-(L9)_{syn})₂ (c). Adapted with permission from ref. 80.

Highlight

1.972 Å indicative of a LS with diamagnetic properties. Under light-irradiation control, $\text{Fe}^{\text{II}}_2(\text{c-L9})_3$ was prepared and exhibited paramagnetism and SCO behaviour (approximately 30% HS, estimated from the $\chi_{\text{M}}T$ value at 300 K), indicating that the ligand field strength of *c*-(L9) differs from that of *o*-(L9)_{anti}, thereby affecting the magnetic properties of those two conformers. The UV/vis spectra of $\text{Fe}^{\text{II}}_2(\text{o-L9})_{\text{anti}3}$ are recorded upon irradiation using $\lambda = 365$ nm light to examine its *in situ* photo-responsive properties. The incomplete conversion from $\text{Fe}^{\text{II}}_2(\text{o-L9})_{\text{anti}3}$ to $\text{Fe}^{\text{II}}_2(\text{c-L9})_3$ was observed under a long irradiation time (on the order of days), which indicates a low conversion efficiency. The conversion from $\text{Fe}^{\text{II}}_2(\text{c-L9})_3$ to $\text{Fe}^{\text{II}}_2(\text{o-L9})_{\text{anti}3}$ was completed in min without decomposition, thereby confirming a quasi-reversible transformation between $\text{Fe}^{\text{II}}_2(\text{o-L9})_{\text{anti}3}$ and $\text{Fe}^{\text{II}}_2(\text{c-L9})_3$. DFT calculations were conducted to estimate the structural changes of $\text{Fe}^{\text{II}}_2(\text{c-L9})_3$. The calculated energy of $\text{Fe}^{\text{II}}_2(\text{c-L9})_3$ was observed to be higher than that of $\text{Fe}^{\text{II}}_2(\text{o-L9})_{\text{anti}3}$ by 48.5 kcal mol⁻¹, which is indicative of the apparent structural changes of $\text{Fe}^{\text{II}}_2(\text{c-L9})_3$ in comparison with that of $\text{Fe}^{\text{II}}_2(\text{o-L9})_{\text{anti}3}$. However, the lack of crystal data of $\text{Fe}^{\text{II}}_2(\text{c-L9})_3$ limits to gain deep insight on the influence of diarylethene conformers on ligand field around Fe^{II} . Under thermodynamic control and in the presence of indispensable $[\text{Fe}^{\text{III}}(\text{Tp}^*)(\text{CN})_3]^-$, $\text{Fe}^{\text{II}}_2(\text{o-L9})_{\text{anti}3}$ and $\text{Fe}^{\text{II}}_2(\text{c-L9})_3$ transformed into tetranuclear square complex $\text{Fe}^{\text{III}}_2\text{Fe}^{\text{II}}_2(\text{o-L9})_{\text{syn}2}$, where alternating Fe^{III} and Fe^{II} ions were bridged by cyano moieties with the $\text{Fe}^{\text{III}}\text{--Fe}^{\text{II}}$ distances of 4.988 and 5.029 Å, respectively, and the diagonal Fe^{II} sites were bridged by two L9 molecules in a parallel conformation. Even at 293 K, the average $\text{Fe}^{\text{II}}\text{--N}$ bond length was still smaller than 2.0 Å in agreement with a LS $\text{Fe}^{\text{II}}\text{--N}$ bond length. Magnetic properties revealed the occurrence of a complete SCO behaviour at $T_{1/2} = 353$ K in $\text{Fe}^{\text{III}}_2\text{Fe}^{\text{II}}_2(\text{o-L9})_{\text{syn}2}$, and the gradual spin transition upon cooling was due to solvent release.

So far, the challenge of SCO molecules based on diarylethene photochromes *via* SCSC transformation is owing to strong absorption of the complexes in the UV region and a very limited light penetration depth into the crystals.⁸⁰

3.2. Structural transformations *via* photochemical [2 + 2] cycloaddition

Photomechanical motions triggered by [2 + 2] cycloaddition reaction where the parallel olefin groups satisfy Schmidt's topochemical criteria⁸⁵ to undergo photoinduced structural transformation have been explored in single molecular magnetism.^{86–88} Still, the photochemical [2 + 2] cycloaddition reaction coupled with SCO has long been a blank area due to the challenge in the tough design of systems accommodating enough space for the deformation of the ligands.

A pioneering work was demonstrated recently for two solvent-free SCO frameworks, $[\text{Fe}(\text{4-spy})_2(\text{Ag}(\text{CN})_2)_2]$ (**29**, 4-spy = 4-styrylpyridine) and $[\text{Fe}(\text{2,4-bpe})_2(\text{Ag}(\text{CN})_2)_2]$ (**30**, 2,4-bpe =

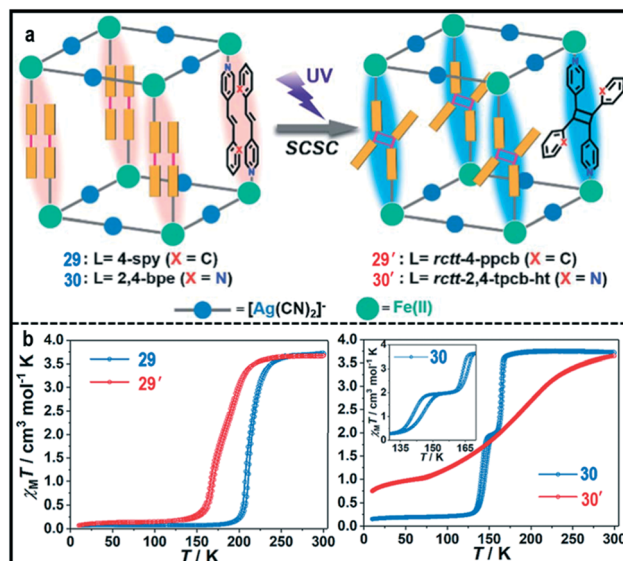


Fig. 12 Strategy for the incorporation of a photochemical [2 + 2] cycloaddition into SCO Hofmann-type frameworks (a) and magnetic susceptibility data for **29** (blue) and **30** (blue) and their photochemical [2 + 2] cycloaddition products **29'** (red) and **30'** (red) (b). Adapted with permission from ref. 82.

trans-1-(2-pyridyl)-2-(4-pyridyl)ethylene).⁸² Both frameworks undergo a quantitative SCSC photodimerization as parallel ethylene groups paired into their cyclobutane counterparts to produce $[\text{Fe}(\text{rctt-4-ppcb})[\text{Ag}(\text{CN})_2]_2]$ (**29'**, rctt-4-ppcb = rctt-1,3-bi(4-pyridyl)-2,4-bis(phenyl)cyclobutane, r = reference group, c = *cis* and t = *trans*) and $[\text{Fe}(\text{rctt-2,4-tpcb-ht})[\text{Ag}(\text{CN})_2]_2]$ (**30'**, rctt-2,4-tpcb-ht = rctt-1,3-bis(2-pyridyl)-2,4-bis(4-pyridyl)cyclobutane, ht = head to tail) (Fig. 12a). During the whole irradiation process, single crystals of **29** remained intact with the crystal colour changed from orange to light grey and the dimerization of 4-spy resulted in a transformation from 2D interdigitated layers to a 3D interpenetrated structure. While single crystals of **30** were cracked into the crystal phase pieces with colour change from orange to light grey. Additionally, a 3D/3D structural transformation accompanied with $\text{Ag}^{\text{I}}\text{--N}$ bond breaking is achieved *via* a photochemical cycloaddition reaction of 2,4-bpe in **30**. More importantly, by the photochemical [2 + 2] cycloaddition reaction, SCO behaviours are dramatically modulated in the shape and the transition temperature (Fig. 12b). The SCO curve of **29'** is more gradual and occurs at a lower temperature compared to that of **29**. In contrast to one-step hysteresis ($T_{1/2}^{\downarrow} = 212$ K and $T_{1/2}^{\uparrow} = 215$ K) of **29**, two-step hysteretic SCO ($T_{1/2}^{\downarrow} = 190$ K, $T_{1/2}^{\uparrow} = 194$ K, $T_{1/2}^{\downarrow} = 166$ K and $T_{1/2}^{\uparrow} = 169$ K) without an obvious plateau is observed in **29'**. For **30'**, an incomplete, gradual and one-step SCO ($T_{1/2} = 162$ K) without hysteretic loop is observed, which is dramatically different from the complete, abrupt, and two-step SCO hysteretic behaviour with ($T_{1/2}^{\downarrow} = 164$ K, $T_{1/2}^{\uparrow} = 167$ K, $T_{1/2}^{\downarrow} = 141$ K and $T_{1/2}^{\uparrow} = 146$ K) in **30**. Magneto-structural correlation demonstrates that **29'** possesses the weaker ligand field where the $\text{Fe}\text{--N}_{\text{av}}$ distance (2.181 Å) is longer and the $\text{Fe}\text{--N}\text{--C}$ angle (164.4°) is

smaller than those of **29** (2.157 Å and 165.4°). Additionally, during the change from an ethylene group to a cyclobutane ring, the π -accepting ability is decreased in **29'**, leading to a reduced ligand field. So the combination of the structural and electronic effects support the lower spin transition temperature in **29'**. In case of **30** \rightarrow **30'**, the cycloaddition reaction makes the decrease of the Fe–N_{av} distance ($d_{\text{Fe–N}_{\text{av}}} = 2.174$ Å (**30**) and 2.154 Å (**30'**)) and the increase of Fe–N–C and C–Ag–C angle ($\angle\text{Fe–N–C}$: 164.7° (**30**) and 168.8° (**30'**), $\angle\text{C–Ag–C}$: 158.2° (**30**) and 175.9° (**30'**)), providing a stronger ligand field in favour of increasing $T_{1/2}$. While the decreased π -accepting ability in **30'** results in a weaker ligand field with the tendency of decreasing the $T_{1/2}$ value. It is competition between the electronic and structural effects that results in the small change of $T_{1/2}$ from **30** to **30'**. As for the cooperativity, the contribution to the SCO cooperativity from weaker $\pi\cdots\pi$ interactions after the cycloaddition reaction outcompetes the formation of the flexible linker and results in the gradual SCO in **29'** and **30'**. Besides the loss of the Ag–N_{py} bond also decreases the SCO cooperativity for **30'**. Therefore, not only the transition temperatures but also the SCO profile can be effectively adjusted by the photochemical [2 + 2] cycloaddition reaction.

Lately, Garcia's group studied the [2 + 2] photodimerization properties of *p*-sulfocinnamic acid (psca) and its inorganic–organic hybrid materials [Fe(H₂O)₆](psca)₂·2H₂O (**31**).⁸⁹ The crystal structure of **31** shows accordance with the Schmidt's topochemical rules of [2 + 2] photodimerization. Replacement of ligand water molecules in such aqua complexes by another suitable ligand can allow [Fe(H₂O)₆](psca)₂·2H₂O to be a precursor of a number of Fe^{II} coordination complexes. For instance, [Fe(DMPP)₂(psca)₂] (DMPP = dimethyl-1-(2'-pyridyl)-pyrazole) using [Fe(H₂O)₆](psca)₂·2H₂O as an intermediate reagent where six water ligands was replaced by two bidentate DMPP ligands and two anionic psca ligands.⁹⁰ This exciting perspective holds a great significance as it opens up an avenue of possibilities to design photoresponsive SCO materials based on psca.

4. Cation-centre-exchange induced SCSC transformations

Metal-centre exchange is a promising tool for synthesis and modification of materials.⁹¹ So far, most of the reported SCSC metal-centre exchange examples were concentrated on the area of porous MOFs materials by post-synthetic modification (PSMs) due to the merits of intrinsic crystallinity and porous nature. Since Sieber *et al.* reported a pioneering work of a thermal spin-transition for the [Co(bpy)₃]²⁺ complex in [Co(bpy)₃][LiCr(ox)₃] (ox = C₂O₄²⁻; bpy = 2,2-bipyridine),⁹² great efforts were made to insert some magnetic bistable molecules within the channels of a 3D magnetic MOF.⁹³ More recently, the solid-state incorporation of a mononuclear LS Fe^{III} complex with the formula [Fe^{III}(sal₂-trien)]NO₃·H₂O (**32**) (H₂sal₂-trien = *N,N'*-disalicylidene-triethylenetetramine) into the large pores (*ca.* 2.2 nm) of a Mn^{II}–Cu^{II} 3D MOF of the

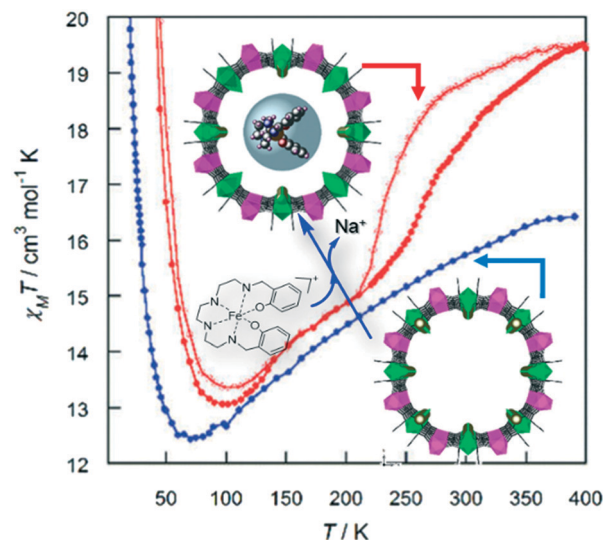


Fig. 13 Schematic representation of the cation exchange SCSC process leading to the hybrid Fe(sal₂-trien)@33 and magnetic properties of **33** and Fe(sal₂-trien)@33. Adapted with permission from ref. 94.

formula Na₄{Mn₄[Cu₂(Me₃mpba)₂]₃}·60H₂O (**33**) [Me₃mpba⁴⁻ = *N,N'*-2,4,6-trimethyl-1,3-phenylenebis(oxamate)] in a SCSC process leads to the formation of a new hybrid SCO material, [Fe^{III}(sal₂-trien)]Na₃{Mn₄[Cu₂(Me₃mpba)₂]₃}·43H₂O (Fe(sal₂-trien)@33) (Fig. 13).⁹⁴ According to unit cell measurements, crystals of Fe(sal₂-trien)@33 appear to be stable upon dehydration. Besides, a small increase in the size of the unit cell is observed for a single crystal of Fe(sal₂-trien)@33 compared with the crystal data of **33**. More importantly, Fe(sal₂-trien)@33 hosted in the pores shows a reversible 5/2 \leftrightarrow 1/2 SCO behaviour revealed from magnetic susceptibility and Mössbauer spectroscopy measurements, which is in contrast to what is seen in the starting precursor salt with the population of LS in the range of 2–300 K.

By contrast, SCSC metal-centre exchange phenomena are scarce in molecular materials. The most challenge is the relatively dense packing as well as the poor crystallinity without the mother liquid. Metal–organic cages with connected pores between cages provide the possibility to perform SCSC metal-centre exchange.^{95–97} It was only recently that such a goal was achieved in the tetrahedral cages [M₄(L10)₆](BF₄)₈ (M = Fe^{II} (**34**), Ni^{II} (**35**); L10 = 1,8-di((imidazol-2-ylmethylene)-1-phenylethanamine)octane).⁹⁸ Cages **34** and **35** were isostructural, where four M^{II} centres occupy the vertices of a tetrahedron and six L10 ligands define the edges. When immersed the single crystals of cage **34** in the Ni(BF₄)₂ solution for one week, no metal-centre exchange phenomena were observed as the form and colour of **34** remained originally. On the contrary, it is of great interest that the colour of crystals gradually changed after soaking cage **35** in the Fe(BF₄)₂ solution (Fig. 14a). Single crystals of FeNi-1 (yellow), FeNi-2 (red), and FeNi-3 (dark purple) were formed after adsorption of Fe^{II} ions for 10 h, 2 days, and 5 days, respectively (Fig. 14b). It is indicative of the occurrence

Highlight

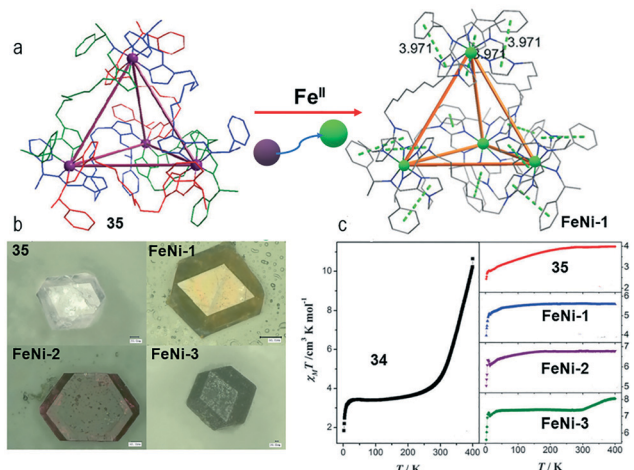


Fig. 14 Representation of metal-centre exchange from the Ni cage to the FeNi-1 cage (a); optical microscopic photographs of colour change of SCSC transformation in the metal-centre exchange process **35** → **FeNi-1** → **FeNi-2** → **FeNi-3** (b) and plots of $\chi_M T$ vs. T for **34**, **35**, **FeNi-1**, **FeNi-2**, and **FeNi-3** (c). Adapted with permission from ref. 98.

of metal-exchange-induced SCSC transformation. The key to this distinction lies in the fact that crystal packing in cage **35** forms an interconnected 3D supramolecular network with 1D channels of *ca.* 9.1 Å along *a* axis providing a pathway for metal-centre exchange. The magnetic susceptibilities of polycrystalline samples of metal-organic cages revealed a different thermal evolution. Along with the increase in the amount of Fe^{II} ions in the FeNi cage, partial Fe^{II} centres of the **FeNi-3** cage can be induced to display SCO behaviour (Fig. 14c).

5. Redox-induced SCSC transformations

In designing multifunctional SCO materials for potential switches, a new approach is the development of a system incorporating a redox-active bridging ligands to control the Fe^{II} SCO transition. Tetrathiafulvalene (TTF), a sulphur-rich conjugated molecule possessing two reversible and easily accessible oxidation states (*i.e.*, radical TTF^{•+} and diamagnetic TTF²⁺), represents a potential linker to spin carriers.^{99,100} Chemical oxidation of the frameworks *via* iodine doping leads to pronounced variations the magnetic properties as witnessed by two new Fe^{II}-based MOFs, {[Fe(dca)][TTF(py)₄]-ClO₄·CH₂Cl₂·2CH₃OH}_{*n*} (**36**), and the I₂-doped analogue of {[Fe(dca)][TTF(py)₄]-0.5I₂·ClO₄·CH₂Cl₂·CH₃OH·C₆H₁₂}_{*n*} (**36@I₂**) (dca = dicyanamide, TTF(py)₄ = tetra(4-pyridyl)tetrathiafulvalene) (Fig. 15).¹⁰¹ When immersed crystal **36** in a solution of iodine in cyclohexane, SCSC transformations was observed accompanied with the colour of crystal changing from red to dark (Fig. 15a). The central C=C bond of the TTF units is 1.41(2) Å in **36@I₂**, which is longer than that of **36**, indicative of the TTF moiety in its radical cation state. A significant aspect of this work was the potential to modulate the magnetic properties of frameworks

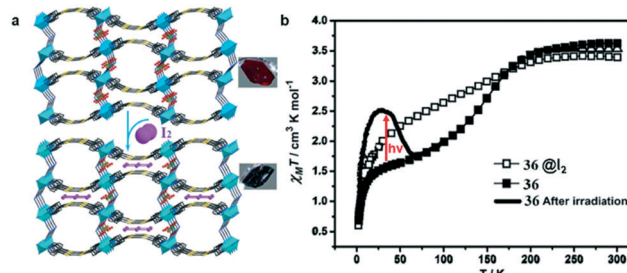


Fig. 15 SCSC transformation (a) and $\chi_M T$ (T) plots for **36** and **36@I₂** (b). Adapted with permission from ref. 101.

via redox state switching (Fig. 15b). In the case of **36** and **36@I₂**, magnetic studies showed that the latter undergoes gradual and incomplete SCO behaviour as does its parent framework **36**. However, the shape of the $\chi_M T$ plot changes significantly upon oxidation. Moreover, the LIESST effect of sample **36** was absent after doping with I₂. Given that oxidation of the TTF core to TTF^{•+} affects the ligand field around the Fe^{II} centre, it is clear that such redox-state modulation is closely related to the magnetic properties.

6. Conclusions

The present highlight exceptionally focuses on the modulation of SCO performance *via* SCSC transformations. To date, SCSC transformations at the porous materials are well-known and investigated elaborately, but SCSC transformations at the discrete molecule still remain less explored. This highlight introduced the latest examples of SCSC-induced SCO upon a different mode of external stimuli (heat, light, solvent, ion exchange as well as redox) and most importantly, illustrated the power of manipulating supramolecular interactions in modifying SCO properties through SCSC transformation. From the standpoint of synthesis, it seems impossible or difficult to design a novel system to explore its SCSC and further investigation of SCO. It is however likely that SCSC transformations are more prone when complexes incorporate guest molecules as well as counterions in the crystal lattice or bound to the metal centre.

Solvent-release induced SCSC transformations were found for complexes **1–13**, in which these were accompanied with the alternation of coordination environment, dimensionality, crystal symmetry, supramolecular isomerization as well as supramolecular interaction. Additionally, non-porous selective magnetic sensors based on **14–21** could be used to identify some volatile alcohols and toxic gases to open up perspectives for further development of iron materials as potential optical-magnetic sensors. Both single- and two-step SCO behaviours have been demonstrated, and the nature of various phases involved has been investigated. In cases of **5** and **6**, the intermediate phase between the LS and HS extremes has also been identified as a result of the disordered ligands or counter anions. In the aspect of light-induced SCSC transformations, photoinduced cyclization SCO systems based on diarylethene

photochromes should be able to undergo photoinduced spin state switching in the solid state, preferably at room temperature. Taken into consideration of the structural fatigability of SCO solids, molecular design of such interesting switchable coordination materials must be rationalized with a high number of switching cycles and with low depreciation.⁶⁹ The photochemical [2 + 2] cycloaddition reaction which can induce drastic changes of structural dimensionality, electronic conjugation and supramolecular interactions, should be extended widely to open up a new area in the designing of photo-responsive magnetic materials. Finally, grafting TTF on SCO-active sites provides a unique and highly useful approach for exploiting redox switchable and multi-stimuli switchable materials.

With those in mind, SCO crystalline materials driven by all above fruitful results of SCSC transformation, will not only continue to serve as a diverse platform for fundamental research, but is expected to hold great prospective to become core elements in intelligent devices.

Conflicts of interest

There are no conflicts to declare.

Acknowledgements

We thank the Fond National de la Recherche Scientifique – FNRS fellowships of chargé de Recherches (28109061 and 24918505); the initial founding of Zhejiang Sci-Tech University (11432932611902 and 11432932612014) and FNRS (CDR 33694457, PDR T.0095.21).

References

- G. Molnár, S. Rat, L. Salmon, W. Nicolazzi and A. Bousseksou, *Adv. Mater.*, 2017, **30**, 1703862.
- Y.-S. Meng and T. Liu, *Acc. Chem. Res.*, 2019, **52**, 1369–1379.
- E. Coronado, *Nat. Rev. Mater.*, 2020, **5**, 87–104.
- T. Zhao, I. Boldog, V. Spasojevic, A. Rotaru, Y. Garcia and C. Janiak, *J. Mater. Chem. C*, 2016, **4**, 6588–6601.
- P. Gütllich, A. B. Gaspar and Y. Garcia, *Beilstein J. Org. Chem.*, 2013, **9**, 342–391.
- R. W. Hogue, S. Singh and S. Brooker, *Chem. Soc. Rev.*, 2018, **47**, 7303–7338.
- B. Li, R.-J. Wei, J. Tao, R.-B. Huang, L.-S. Zheng and Z. Zheng, *J. Am. Chem. Soc.*, 2010, **132**, 1558–1566.
- Z.-P. Ni, J.-L. Liu, M. N. Hoque, W. Liu, J.-Y. Li, Y.-C. Chen and M.-L. Tong, *Coord. Chem. Rev.*, 2017, **335**, 28–43.
- M. J. Murphy, K. A. Zenere, F. Ragon, P. D. Southon, C. J. Kepert and S. M. Neville, *J. Am. Chem. Soc.*, 2017, **139**, 1330–1335.
- H. Hagiwara, T. Masuda, T. Ohno, M. Suzuki, T. Udagawa and K.-I. Murai, *Cryst. Growth Des.*, 2017, **17**, 6006–6019.
- X. Bao, H. J. Shepherd, L. Salmon, G. Molnár, M.-L. Tong and A. Bousseksou, *Angew. Chem., Int. Ed.*, 2013, **52**, 1198–1202.
- L. J. K. Cook, R. Kulmaczewski, O. Cespedes and M. A. Halcrow, *Chem. – Eur. J.*, 2016, **22**, 1789–1799.
- M. M. Dîrtu, A. D. Naik, A. Rotaru, L. Spinu, D. Poelman and Y. Garcia, *Inorg. Chem.*, 2016, **55**, 4278–4295.
- B. Ding, Y. Y. Wang, S. X. Liu, X. X. Wu, Z. Z. Zhu, J. Z. Huo and Y. Y. Liu, *CrystEngComm*, 2015, **17**, 5396–5409.
- Z. Huang, P. S. White and M. Brookhart, *Nature*, 2010, **465**, 598–601.
- Y. Wang, R. Chen, W. Jia, Q. Wang, C.-Y. Xue, J.-H. Fan, W.-R. Qi, Y.-J. Qin, Y.-H. Pan and R.-R. Yang, *Inorg. Chem.*, 2018, **57**, 2381–2385.
- Z.-M. Hao and X.-M. Zhang, *Dalton Trans.*, 2011, **40**, 2092–2098.
- S. M. Neville, G. J. Halder, K. W. Chapman, M. B. Duriska, P. D. Southon, J. D. Cashion, J.-F. Letard, B. Moubaraki, K. S. Murray and C. J. Kepert, *J. Am. Chem. Soc.*, 2008, **130**, 2869–2876.
- K. A. Zenere, S. G. Duyker, E. Trzop, E. Collet, B. Chan, P. W. Doheny, C. J. Kepert and S. M. Neville, *Chem. Sci.*, 2018, **9**, 5623–5629.
- R. Jankowski, M. Reczynski, S. Chorazy, M. Zychowicz, M. Arczynski, M. Koziel, K. Ogorzaly, W. Makowski, D. Pinkowicz and B. Sieklucka, *Chem. – Eur. J.*, 2020, **26**, 11187–11198.
- W. Liu, Y.-Y. Peng, S.-G. Wu, Y.-C. Chen, M. N. Hoque, Z.-P. Ni, X.-M. Chen and M.-L. Tong, *Angew. Chem., Int. Ed.*, 2017, **56**, 14982–14986.
- J. J. Vittal and H. S. Quah, *Coord. Chem. Rev.*, 2017, **342**, 1–18.
- A. Chaudhary, A. Mohammad and S. M. Mobin, *Cryst. Growth Des.*, 2017, **17**, 2893–2910.
- Q.-Q. Li, H. Liu, T.-T. Zheng, P. Liu, J.-X. Song and Y.-Y. Wang, *CrystEngComm*, 2020, **22**, 6750–6775.
- A. Lennartson, M. Håkansson and S. Jagner, *New J. Chem.*, 2007, **31**, 344–347.
- S. Supriya and S. K. Das, *J. Am. Chem. Soc.*, 2007, **129**, 3464–3465.
- M. Reiners, D. Baabe, K. Muenster, M.-K. Zaretske, M. Freytag, P. G. Jones, Y. Coppel, S. Bontemps, I. del Rosal, L. Maron and M. D. Walter, *Nat. Chem.*, 2020, **12**, 740–746.
- W.-B. Chen, Y.-C. Chen, M. Yang, M.-L. Tong and W. Dong, *Dalton Trans.*, 2018, **47**, 4307–4314.
- G. Aromi, L. A. Barrios, O. Roubeau and P. Gamez, *Coord. Chem. Rev.*, 2011, **255**, 485–546.
- Y. Garcia, N. N. Adarsh and A. D. Naik, *Chimia*, 2013, **67**, 411–418.
- J. Olguin and S. Brooker, *Spin-crossover in discrete polynuclear complexes*, John Wiley & Sons Ltd., 2013.
- W.-B. Chen, J.-D. Leng, Z.-Z. Wang, Y.-C. Chen, Y. Miao, M.-L. Tong and W. Dong, *Chem. Commun.*, 2017, **53**, 7820–7823.
- M. Shatruk, H. Phan, B. A. Chrisostomo and A. Suleimenova, *Coord. Chem. Rev.*, 2015, **289–290**, 62–73.
- M. Nihei, L. Han and H. Oshio, *J. Am. Chem. Soc.*, 2007, **129**, 5312–5313.
- V. Jornet-Molla, Y. Duan, C. Gimenez-Saiz, Y.-Y. Tang, P.-F. Li, F. M. Romero and R.-G. Xiong, *Angew. Chem., Int. Ed.*, 2017, **56**, 14052–14056.

- 36 J. E. Clements, P. R. Airey, F. Ragon, V. Shang, C. J. Kepert and S. M. Neville, *Inorg. Chem.*, 2018, **57**, 14930–14938.
- 37 F. Kobayashi, Y. Komatsumaru, R. Akiyoshi, M. Nakamura, Y. Zhang, L. F. Lindoy and S. Hayami, *Inorg. Chem.*, 2020, **59**, 16843–16852.
- 38 L. A. Barrios, C. Bartual-Murgui, E. Peyrecave-Lleixa, B. Le Guennic, S. J. Teat, O. Roubeau and G. Aromi, *Inorg. Chem.*, 2016, **55**, 4110–4116.
- 39 X. Bao, P.-H. Guo, J.-L. Liu, J.-D. Leng and M.-L. Tong, *Chem. – Eur. J.*, 2011, **17**, 2335–2339.
- 40 M. A. Halcrow, *Chem. Soc. Rev.*, 2011, **40**, 4119–4142.
- 41 J. J. M. Amooore, S. M. Neville, B. Moubaraki, S. S. Iremonger, K. S. Murray, J.-F. Letard and C. J. Kepert, *Chem. – Eur. J.*, 2010, **16**, 1973–1982.
- 42 Y.-H. Luo, L.-J. Yang, Q.-L. Liu, Y. Ling, W. Wang and B.-W. Sun, *Dalton Trans.*, 2014, **43**, 16937–16942.
- 43 M. Steinert, B. Schneider, S. Dechert, S. Demeshko and F. Meyer, *Angew. Chem., Int. Ed.*, 2014, **53**, 6135–6139.
- 44 R. G. Miller and S. Brooker, *Chem. Sci.*, 2016, **7**, 2501–2505.
- 45 F.-L. Yang, X. Chen, W.-H. Wu, J.-H. Zhang, X.-M. Zhao, Y.-H. Shi and F. Shen, *Dalton Trans.*, 2019, **48**, 231–241.
- 46 N. Li, J.-P. Xue, J.-L. Liu, Y.-Y. Wang, Z.-S. Yao and J. Tao, *Dalton Trans.*, 2020, **49**, 998–1001.
- 47 P. Gutlich and H. A. Goodwin, *Topics in Current Chemistry*, Spin Crossover in Transition Metal Compounds II, Springer-Verlag, Berlin, 2004.
- 48 H. A. Goodwin, *Top. Curr. Chem.*, 2004, **234**, 23–47.
- 49 D. J. Harding, P. Harding and W. Phonsri, *Coord. Chem. Rev.*, 2016, **313**, 38–61.
- 50 R. G. Miller, S. Narayanaswamy, J. L. Tallon and S. Brooker, *New J. Chem.*, 2014, **38**, 1932–1941.
- 51 D. Shao, L. Shi, L. Yin, B.-L. Wang, Z.-X. Wang, Y.-Q. Zhang and X.-Y. Wang, *Chem. Sci.*, 2018, **9**, 7986–7991.
- 52 D. Shao, L. Shi, F.-X. Shen, X.-Q. Wei, O. Sato and X.-Y. Wang, *Inorg. Chem.*, 2019, **58**, 11589–11598.
- 53 S. Rodriguez-Jimenez, H. L. C. Feltham and S. Brooker, *Angew. Chem., Int. Ed.*, 2016, **55**, 15067–15071.
- 54 J. S. Costa, S. Rodríguez-Jiménez, G. A. Craig, B. Barth, C. M. Beavers, S. J. Teat, K. J. Gagnon, L. A. Barrios, O. Roubeau and G. Aromi, *Inorg. Chem. Front.*, 2020, **7**, 3165–3175.
- 55 J. Cirera, *Rev. Inorg. Chem.*, 2014, **34**, 199–216.
- 56 G. Mínguez Espallargas and E. Coronado, *Chem. Soc. Rev.*, 2018, **47**, 533–557.
- 57 D. Gentili, N. Demitri, B. Schäfer, F. Liscio, I. Bergenti, G. Ruani, M. Ruben and M. Cavallini, *J. Mater. Chem. C*, 2015, **3**, 7836–7844.
- 58 J. Sanchez Costa, S. Rodriguez-Jimenez, G. A. Craig, B. Barth, C. M. Beavers, S. J. Teat and G. Aromi, *J. Am. Chem. Soc.*, 2014, **136**, 3869–3874.
- 59 R.-J. Wei, J. Tao, R.-B. Huang and L.-S. Zheng, *Inorg. Chem.*, 2011, **50**, 8553–8564.
- 60 W. Huang, F. Shen, M. Zhang, D. Wu, F. Pan and O. Sato, *Dalton Trans.*, 2016, **45**, 14911–14918.
- 61 A. D. Naik, K. Robeyns, C. F. Meunier, A. F. Léonard, A. Rotaru, B. Tinant, Y. Filinchuk, B. L. Su and Y. Garcia, *Inorg. Chem.*, 2014, **53**, 1263–1265.
- 62 Y. Guo, S. Xue, M. M. Dirtu and Y. Garcia, *J. Mater. Chem. C*, 2018, **6**, 3895–3900.
- 63 Y. Garcia, in *Advances in Inorganic Chemistry*, ed. D. Ruiz-Molina and R. van Eldik, Academic Press, 2020, vol. 76, pp. 121–153.
- 64 C. Bartual-Murgui, C. Codina, O. Roubeau and G. Aromi, *Chem. – Eur. J.*, 2016, **22**, 12767–12776.
- 65 C. Bartual-Murgui, R. Diego, S. Vela, S. J. Teat, O. Roubeau and G. Aromi, *Inorg. Chem.*, 2018, **57**, 11019–11026.
- 66 G. Aromi, C. M. Beavers, J. Sánchez Costa, G. A. Craig, G. Mínguez Espallargas, A. Orera and O. Roubeau, *Chem. Sci.*, 2016, **7**, 2907–2915.
- 67 A. R. Zuluaga, A. J. Brock, M. C. Pfrunder, W. Phonsri, K. S. Murray, P. Harding, A. S. Micallef, K. M. Mullen, J. K. Clegg, D. J. Harding and J. C. McMurtrie, *Chem. Mater.*, 2020, **32**, 10076–10083.
- 68 S.-G. Wu, M. N. Hoque, J.-Y. Zheng, G.-Z. Huang, N. V. H. Anh, L. Ungur, W.-X. Zhang, Z.-P. Ni and M.-L. Tong, *CCS Chem.*, 2021, **3**, 453–459.
- 69 B. Brachňaková and I. Šalitroš, *Chem. Pap.*, 2018, **72**, 773–798.
- 70 M. M. Khusniyarov, *Chem. – Eur. J.*, 2016, **22**, 15178–15191.
- 71 M.-L. Boillot, C. Roux, J.-P. Audière, A. Dausse and J. Zarembowitch, *Inorg. Chem.*, 1996, **35**, 3975–3980.
- 72 M. L. Boillot, S. Pillet, A. Tissot, E. Rivière, N. Claiser and C. Lecomte, *Inorg. Chem.*, 2009, **48**, 4729–4736.
- 73 Y. Hasegawa, K. Takahashi, S. Kume and H. Nishihara, *Chem. Commun.*, 2011, **47**, 6846–6848.
- 74 Y. Hasegawa, S. Kume and H. Nishihara, *Dalton Trans.*, 2009, 280–284.
- 75 M. Milek, F. W. Heinemann and M. M. Khusniyarov, *Inorg. Chem.*, 2013, **52**, 11585–11592.
- 76 M. Nihei, Y. Suzuki, N. Kimura, Y. Kera and H. Oshio, *Chem. – Eur. J.*, 2013, **19**, 6946–6949.
- 77 B. Rösner, M. Milek, A. Witt, B. Gobaut, P. Torelli, R. H. Fink and M. M. Khusniyarov, *Angew. Chem., Int. Ed.*, 2015, **54**, 12976–12980.
- 78 M. Estrader, J. Salinas Uber, L. A. Barrios, J. Garcia, P. Lloyd-Williams, O. Roubeau, S. J. Teat and G. Aromi, *Angew. Chem., Int. Ed.*, 2017, **56**, 15622–15627.
- 79 M. Moertel, A. Witt, F. W. Heinemann, S. Bochmann, J. Bachmann and M. M. Khusniyarov, *Inorg. Chem.*, 2017, **56**, 13174–13186.
- 80 Z.-Y. Li, J.-W. Dai, M. Damjanović, T. Shiga, J.-H. Wang, J. Zhao, H. Oshio, M. Yamashita and X.-H. Bu, *Angew. Chem., Int. Ed.*, 2019, **58**, 4339–4344.
- 81 M. Mörtel, T. Lindner, A. Scheurer, F. W. Heinemann and M. M. Khusniyarov, *Inorg. Chem.*, 2020, **59**, 2659–2666.
- 82 L.-F. Wang, W.-M. Zhuang, G.-Z. Huang, Y.-C. Chen, J.-Z. Qiu, Z.-P. Ni and M.-L. Tong, *Chem. Sci.*, 2019, **10**, 7496–7502.
- 83 K. Sénéchal-David, N. Zaman, M. Walko, E. Halza, E. Rivière, R. Guillot, B. L. Feringa and M. L. Boillot, *Dalton Trans.*, 2008, 1932–1936.
- 84 Y. Garcia, V. Ksenofontov, R. Lapouyade, A. D. Naik, F. Robert and P. Gülich, *Opt. Mater.*, 2011, **33**, 942–948.

- 85 G. M. J. Schmidt, *Pure Appl. Chem.*, 1971, **27**, 647–678.
- 86 L.-F. Wang, J.-Z. Qiu, Y.-C. Chen, J.-L. Liu, Q.-W. Li, J.-H. Jia and M.-L. Tong, *Inorg. Chem. Front.*, 2017, **4**, 1311–1318.
- 87 L.-F. Wang, J.-Z. Qiu, J.-L. Liu, Y.-C. Chen, J.-H. Jia, J. Jover, E. Ruiz and M.-L. Tong, *Chem. Commun.*, 2015, **51**, 15358–15361.
- 88 M. Feng, Z.-Y. Ruan, Y.-C. Chen and M.-L. Tong, *Chem. Commun.*, 2020, **56**, 13702–13718.
- 89 V. Kumar, L. Fusaro, C. Aprile, K. Robeyns and Y. Garcia, *Cryst. Growth Des.*, 2020, **20**, 7850–7861.
- 90 V. Kumar, M. El-Massaoudi, S. Radi, K. Van Hecke, A. Rotaru and Y. Garcia, *New J. Chem.*, 2020, **44**, 13902–13912.
- 91 W. Meng, H. Li, Z. Xu, S. Du, Y. Li, Y. Zhu, Y. Han, H. Hou, Y. Fan and M. Tang, *Chem. – Eur. J.*, 2014, **20**, 2945–2952.
- 92 R. Sieber, S. Decurtins, H. Stoeckli-Evans, C. Wilson, D. Yufit, J. A. K. Howard, S. C. Capelli and A. Hauser, *Chem. – Eur. J.*, 2000, **6**, 361–368.
- 93 M. Mon, A. Pascual-Álvarez, T. Grancha, J. Cano, J. Ferrando-Soria, F. Lloret, J. Gascon, J. Pasán, D. Armentano and E. Pardo, *Chem. – Eur. J.*, 2016, **22**, 539–545.
- 94 A. Abherve, T. Grancha, J. Ferrando-Soria, M. Clemente-Leon, E. Coronado, J. C. Waerenborgh, F. Lloret and E. Pardo, *Chem. Commun.*, 2016, **52**, 7360–7363.
- 95 R.-J. Wei, Q. Huo, J. Tao, R.-B. Huang and L.-S. Zheng, *Angew. Chem., Int. Ed.*, 2011, **50**, 8940–8943.
- 96 D.-H. Ren, D. Qiu, C.-Y. Pang, Z. Li and Z.-G. Gu, *Chem. Commun.*, 2015, **51**, 788–791.
- 97 L. F. Lindoy, *J. Inclusion Phenom. Macrocyclic Chem.*, 2019, **94**, 121–131.
- 98 F.-L. Zhang, J.-Q. Chen, L.-F. Qin, L. Tian, Z. Li, X. Ren and Z.-G. Gu, *Chem. Commun.*, 2016, **52**, 4796–4799.
- 99 Y.-R. Qiu, L. Cui, P.-Y. Cai, F. Yu, M. Kurmoo, C. F. Leong, D. M. D'Alessandro and J.-L. Zuo, *Chem. Sci.*, 2020, **11**, 6229–6235.
- 100 J. Su, N. Xu, R. Murase, Z.-M. Yang, D. M. D'Alessandro, J.-L. Zuo and J. Zhu, *Angew. Chem., Int. Ed.*, 2021, **60**, 4789–4795.
- 101 H.-Y. Wang, J.-Y. Ge, C. Hua, C.-Q. Jiao, Y. Wu, C. F. Leong, D. M. D'Alessandro, T. Liu and J.-L. Zuo, *Angew. Chem., Int. Ed.*, 2017, **56**, 5465–5470.